JAERI-Tech
2001-066

DESIGN OF IN-VESSEL NEUTRON MONITOR USING MICRO FISSION CHAMBERS FOR ITER

October 2001

Takeo NISHITANI, Katsuyuki EBISAWA, Chris WALKER*
and Satoshi KASAI

日本原子力研究所
Japan Atomic Energy Research Institute

本レポートは，日本原子力研究所が不定期に公刊している研究報告書です。
入手の問合わせは，日本原子力研究所研究情報部研究情報課（〒319－1195 茨城県那珂郡東海村）あて，お申し越しください。なお，このほかに財団法人原子力弘済会資料センター（〒319－1195 茨城県那珂郡東海村日本原子力研究所内）で複写による実費頒布をおこなっております。

This report is issued irregularly.
Inquiries about availability of the reports should be addressed to Research Information Division, Department of Intellectual Resources, Japan Atomic Energy Research Institute, Tokai-mura, Naka-gun, Ibaraki-ken 〒319－1195, Japan.

編集兼発行　日本原子力研究所

JAERI-Tech 2001-066

Design of In-vessel Neutron Monitor using Micro Fission Chambers for ITER

Takeo NISHITANI, Katsuyuki EBISAWA+, Chris WALKER* and Satoshi KASAI

Department of Fusion Engineering Research
(Tokai Site)
Naka Fusion Research Establishment
Japan Atomic Energy Research Institute
Tokai-mura, Naka-gun, Ibaraki-ken

(Received September 12, 2001)

A neutron monitor using micro fission chambers to be installed inside the vacuum vessel has been designed for compact ITER (ITER-FEAT). We investigated the responses of the micro fission chambers to find the suitable position of micro fission chambers by a neutron Monte Carlo calculation using MCNP version 4b code. It was found that the averaged output of the micro fission chambers behind blankets at upper outboard and lower outboard is insensitive to the changes in the plasma position and the neutron source profile. A set of ^{235}U micro fission chamber and "blank" detector which is a fissile material free detector to identify noise issues such as from γ-rays are installed behind blankets. Employing both pulse counting mode and Campbelling mode in the electronics, the ITER requirement of 10^7 dynamic range with 1 ms temporal resolution can be accomplished. The in-situ calibration has been simulated by MCNP calculation, where a point source of 14 MeV neutrons is moving on the plasma axis. It was found that the direct calibration is possible by using a neutron generator with an intensity of 10^{11} n/s. The micro fission chamber system can meet the required 10% accuracy for a fusion power monitor.

Keywords: Neutron Monitor, Micro Fission Chamber, ITER, Fusion Power, Campbelling Mode, MCNP, Neutron Source Strength

---

This work is conducted as an ITER Engineering Activities as this report corresponds to ITER Design Task Agreement on "Diagnostics Design" (N 55 TD 02.03FJ).

+ Department of ITER Project (Present address: Toshiba Corp.)

* ITER Joint Central Team, Garching

マイクロフィッションチェンバーを用いたITER用真空容器内中性子モニターの設計

日本原子力研究所那珂研究所核融合工学部
西谷　健夫・海老澤　克之+・Chris WALKER*・河西　敏

(2001年9月12日受理)

マイクロフィッションチェンバーを用いたコンパクトITER（ITER-FEAT）用の真空容器内中性子モニターの設計を行った。マイクロフィッションチェンバーを取付けるための最適な位置を決定するため、中性子モンテカルロコードMCNP-4bを用いて、マイクロフィッションチェンバーの応答を計算した。その結果、外側上部及び下部の遮蔽ブランケットモジュールの裏面にマイクロフィッションチェンバーを取付け、その出力の平均を取ることによって、プラズマ位置や中性子発生分布の変化の影響を受けずに中性子発生量を測定できることを明らかにした。またγ線等によるノイズを評価するために、^{235}Uを含むマイクロフィッションチェンバーと核分裂物質を含まないダミーチェンバーを併せてブランケット裏面に取付けることとした。信号処理ではパルス計数方式とキャンベル方式を併用することによって、ITERの要求仕様である10^7のダイナミックレンジと1msの時間分解能を達成できることを示した。またマイクロフィッションチェンバーのその場較正試験は、10^{11} n/sの強度中性子発生装置を真空容器内で移動させることにより可能であることを、MCNP計算により示した。これらの検討により、この中性子モニターはITERの要求精度10%を満足することを明らかにした。

本研究はＩＴＥＲ工学設計活動の一環として実施したもので、本報告は設計タスク協定(N 55 TD02. 03FJ)に基づくものである。

那珂研究所（東海駐在）：〒319-1195 茨城県那珂郡東海村白方白根2-4
+　ITER開発室（現（株）東芝）
*　ITERガルヒンク共同センター

Contents

1.Introduction 1
1.1 Functions 1
1.2 Design Requirements 1
2. Conceptual Design Description 2
2.1 Micro Fission Chamber 2
2.2 Installation Position 6
2.3 Effects of Plasma Position and Neutron Source Profile 13
2.4 Lifetime Estimation 20
2.5 Dynamic Range 22
2.6 Gamma-ray Effect 24
2.7 Magnetic Field Effect 25
2.8 Nuclear Heating 25
2.9 Calibration 26
3. Detailed System Description 31
3.1 General Equipment Arrangement 31
3.2 Micro Fission Chamber Unit 31
3.3 Installation of Micro Fission Chambers on Vacuum Vessel 31
3.4 Data Acquisition and Control 39
3.5 Calibration Hardware 41
3.6 Component List 41
4. Operation State Description 42
4.1 Commissioning State 42
4.2 Calibration State 42
4.3 Experimental Operations State 42
4.4 Maintenance State 42
5. Critical Design Areas and R&D Items 43
5.1 Critical Design Areas 43
5.2 Necessary R&D Items 43
6. Conclusion 44
Acknowledgments 45
References 46
Appendix 48

目　次

1 序　論 1
1.1 機能 1
1.2 設計要求事項 1
2. 概念設計 2
2.1 マイクロフィッションチェンバー 2
2.2 設置位置 6
2.3 プラズマ位置及び中性子発生分布の影響 13
2.4 寿命評価 20
2.5 測定範囲 22
2.6 γ線の影響 24
2.7 磁場の影響 25
2.8 核発熱 25
2.9 較正 26
3. システム詳細設計 31
3.1 装置の全体配置 31
3.2 マイクロフィッションチェンバーユニット 31
3.3 マイクロフィッションチェンバーの真空容器への取付け 31
3.4 データ処理及び制御 39
3.5 較正用機器 41
3.6 構成要素リスト 41
4. 運転状況 42
4.1 装置組立て期間 42
4.2 較正試験期間 42
4.3 実験運転期間 42
4.4 装置保守期間 42
5. 主要設計領域とR&D項目 43
5.1 主要設計領域 43
5.2 R&D項目 43
6. 結　論 44
謝　辞 45
参考文献 46
付　録 48

1. INTRODUCTION

1.1 Functions

The micro fission chamber is the candidate diagnostic to measure the fusion power, which is one of the basic control parameters. In present large tokamaks such as JET[1], TFTR[2] or JT-60U[3], the neutron yield measurement has been carried out using ^{235}U or ^{238}U fission chambers installed outside the vacuum vessel. Detection efficiencies of those detectors are easily affected by surrounding equipment such as other diagnostics or heating systems. ITER has thick components such as blanket and vacuum vessel, so that detectors outside the vacuum vessel can not measure the neutron source strength with sufficient accuracy. We are designing micro fission chambers, which are pencil size gas counters with fissile material inside, to be installed in the vacuum vessel as neutron flux monitors for ITER[4-8]. By installing the detectors at several poloidal angles, this neutron monitor may reject or reduce the error of the neutron yield caused by the change of the plasma position and/or shape. This report provides the technical feasibility of the neutron monitor system for compact ITER (ITER-FEAT).

1.2 Design Requirements

Target values of the design requirements for the Micro fission Chamber (5.5.B.03) are listed in Table 1.2-1. So the neutron detector has to have wide dynamic range and fast response. From the technical point of view, it should be robust in the ITER environment such as radiation, electro-magnetic noises, and mechanical vibrations, and not sensitive to gamma-rays. The detection efficiency should be maintained in the ITER operation life, and the detectors should be calibrated easily. In ITER, conventional neutron monitors installed outside the vacuum vessel (WBS 5.5.B.04) and in-vessel neutron monitor using micro fission chamber are proposed for the neutron yield measurement.

Table 1.2-1 Target Values of Design Requirements

Total Neutron Flux				
Parameter	Parameter range	Spatial Resolution	Time Resolution	Accuracy
Total neutron flux	10^{14}-10^{21} n s^{-1}	integral	1 ms	10%
Fusion power	≤1 GW	integral	1 ms	10%

2. CONCEPTUAL DESIGN DESCRIPTION

2.1 Micro Fission Chamber

A micro fission chamber is a pencil size gas counter with fissile material inside, which was developed as an in-core monitor of the fission reactor. Figure 2.1-1 shows the schematics of the typical micro fission chamber with wide dynamic range, which is commercially available. We should add a sheath for the chamber from two reasons for use in ITER. One is to shield electro-magnetic noises. Another is safety reason. The sheath will prevent the uranium contamination inside the vacuum vessel when the uranium leaks from the chamber housing. The sheath should include a thermal neutron shield with 1-mm thick cadmium. In this detector, about 12 mg of UO_2 is coated on the cylindrical electrode and 14.6 atm of Ar + 5% N_2 gas is filled between the electrodes.

The micro fission chamber can be operated with pulse counting mode at low neutron flux, Campbelling (mean square voltage) mode[9] at medium flux and current mode at high flux. Combination of those operation modes may provide wide dynamic range of 10^{10} with the temporal resolution of 1 ms, which satisfies the ITER requirement. The most popular candidates of the fissile material in the micro fission chamber are ^{235}U, ^{238}U and ^{232}Th. ^{235}U has large fission cross-section for thermal neutrons and others cause fission event only for fast neutrons higher than ~0.8 MeV. The fission cross-section of ^{232}Th is several times lower than that of ^{238}U. So we employ ^{235}U as the fissile material for the micro fission

chamber to obtain sufficient counting rate. The fission cross-section of ^{235}U is shown in Fig.2.1-2. The typical performance of the micro fission chamber of ^{235}U with the dimension shown in Fig.2.1-1 is listed in Table 2.1-1.

Table 2.1-1 Performance of the micro fission chamber of ^{235}U.

Diameter	14 mm
Active length	76 mm
Fissile material Fissile material density Total amount	^{235}U 0.6 mg $(UO_2)/cm^2$ total 12 mg of UO_2
Ionizing gas	14.6 atm of Ar + 5% N_2
Housing material	Stainless steel 316L
Neutron sensitivity for fission reactor spectrum Pulse counting mode MSV mode DC mode	 2.2×10^{-3} cps/nv 5.7×10^{-28} A^2/Hz/nv 4.6×10^{-15} A/nv
Gamma sensitivity MSV mode DC mode	 7.72×10^{-29} A^2/Hz/R/h 1.54×10^{-12} A/R/h

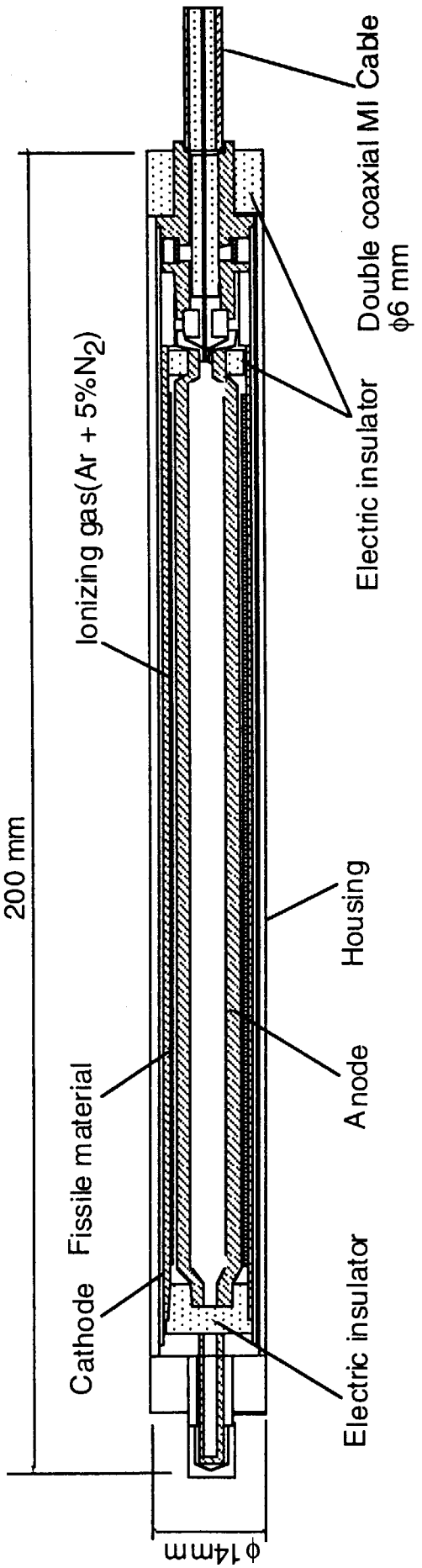

Figure 2.1-1 Schematics of micro fission chamber

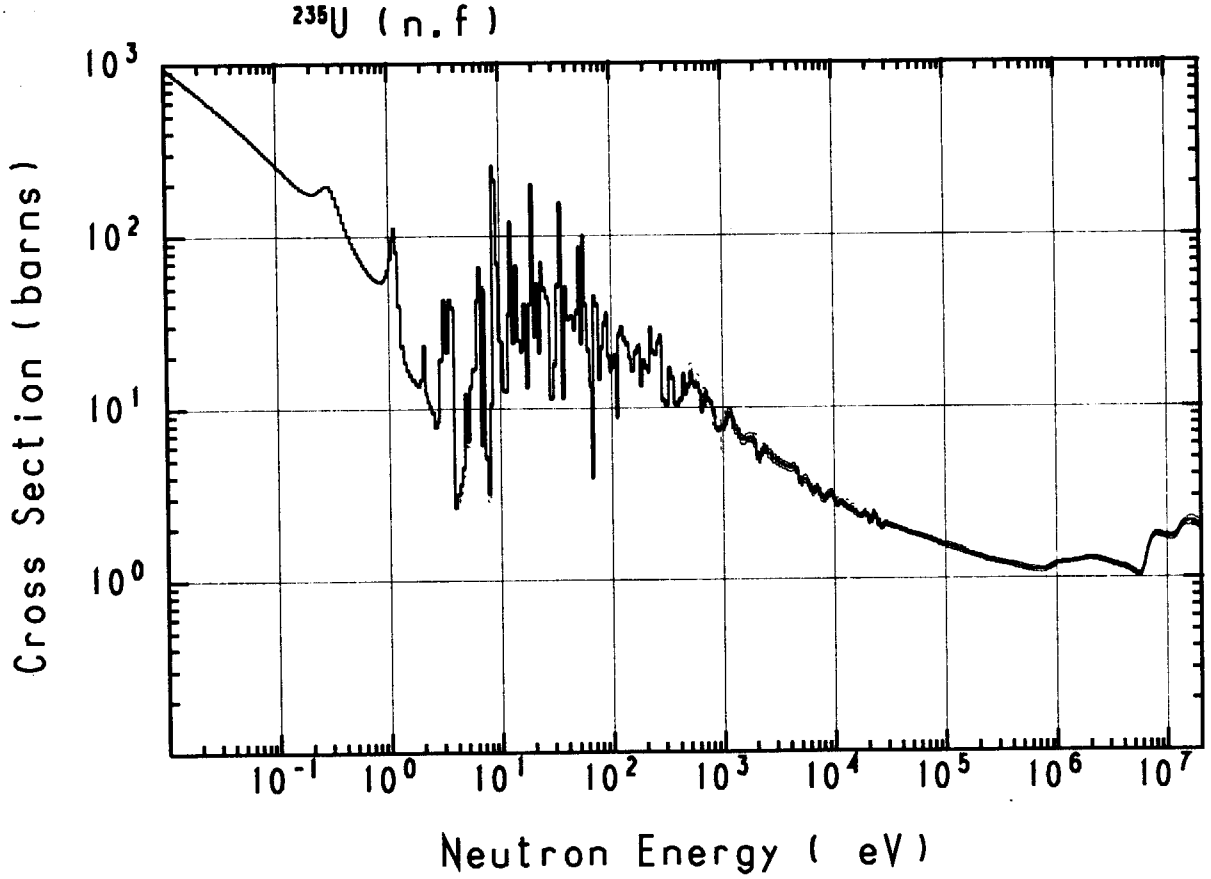

Figure 2.1-2 Fission cross-section of ^{235}U as a function of neutron energy.

2.2 Installation Position

2.2.1 Candidate of installation position

In ITER-FDR, we have a plan to install micro fission chambers on the front side of the back plate in the gap between adjacent blanket modules and behind the blankets at 10 poloidal locations. The neutron flux in the gap between adjacent blanket modules was about 1 order higher than that behind the blankets, which means that streamed neutrons were dominant in the gap. So a change of the gap width due to a thermal expansion or mechanical movements would change the neutron flux. Therefor we eliminate the install in the gap.

For ITER-FEAT, we have two ideas of the installation position as shown in Figure 2.2-1. One is behind shielding blankets, and another is backside of filler module. Arrangement of the micro fission chambers on filler modules is shown in Fig.2.2-2.

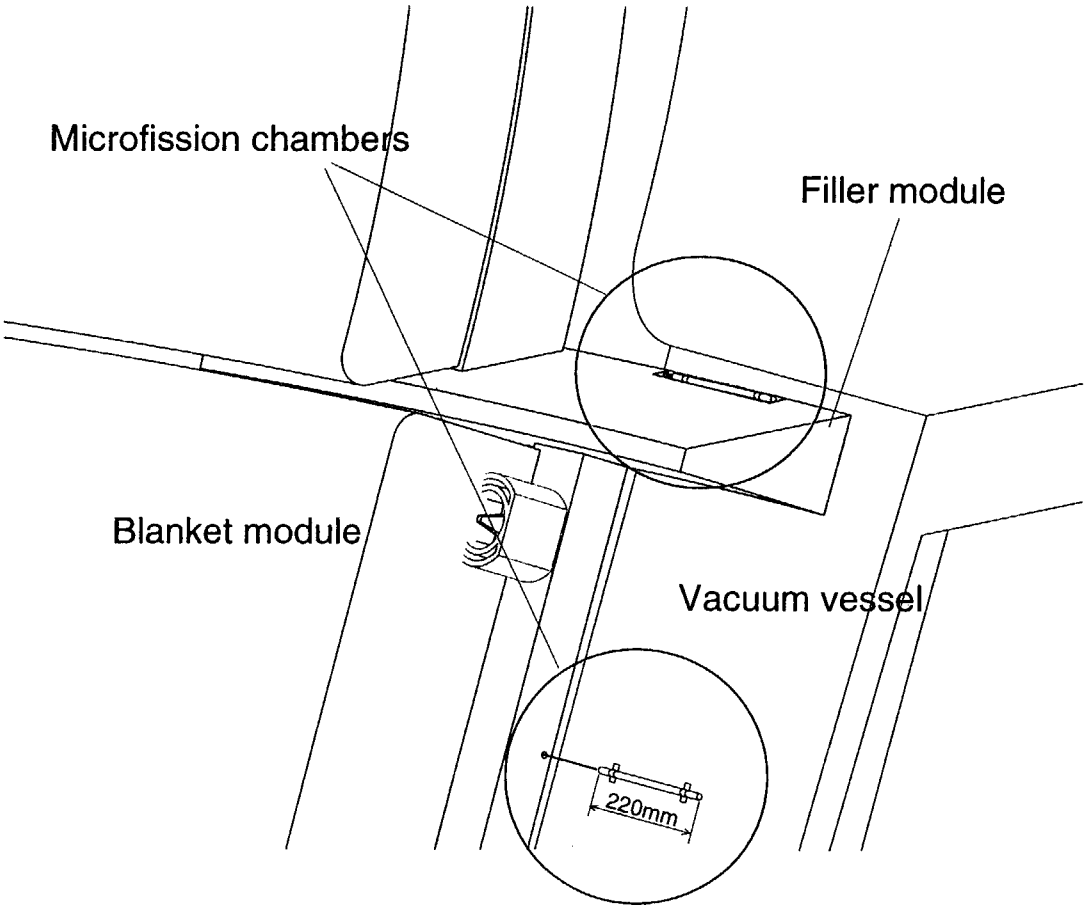

Figure 2.2-1 Candidate of the micro fission chamber location.

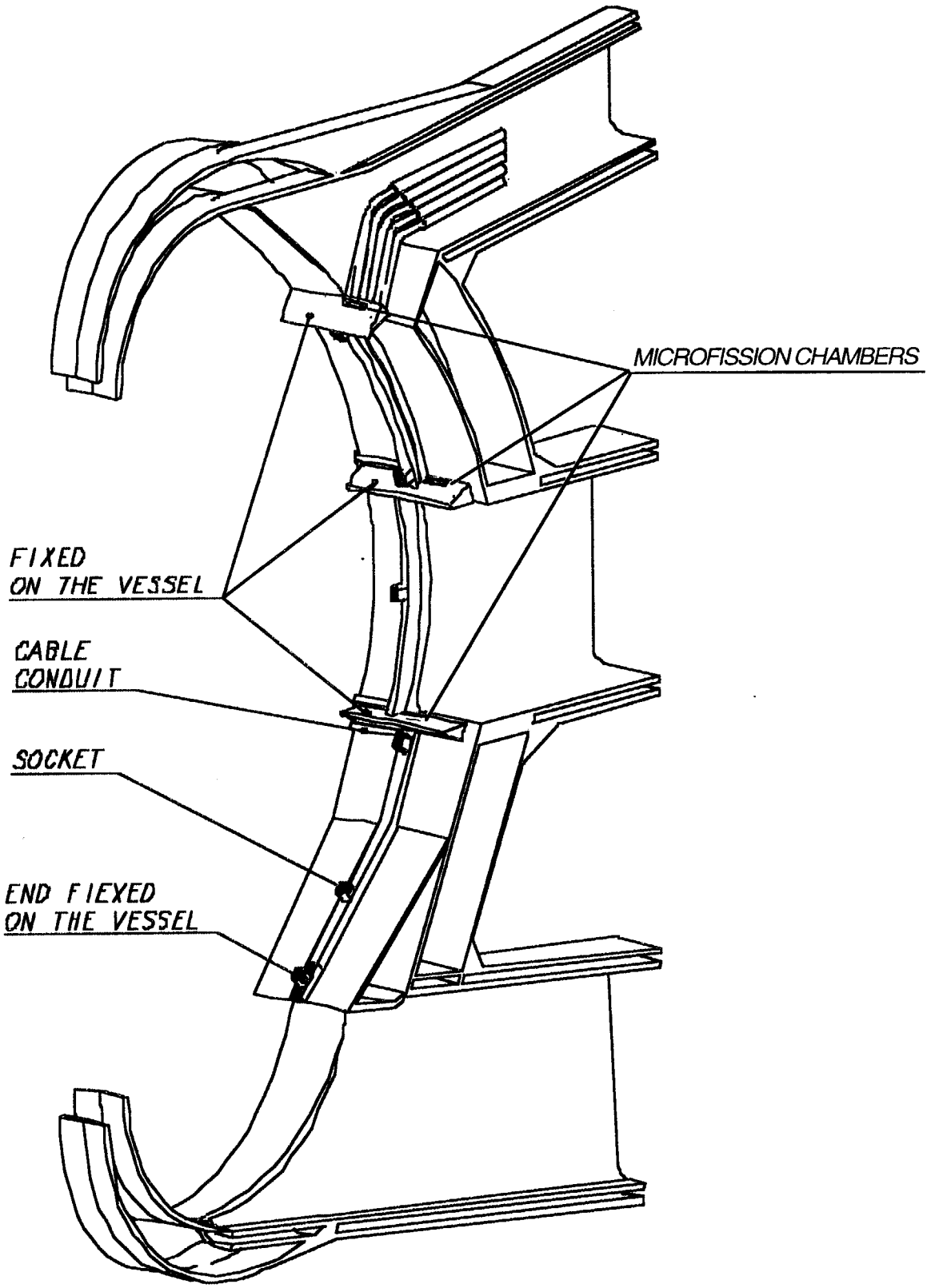

Figure 2.2-2 Arrangement of micro fission chambers on filler modules.

2.2.2 Neutronics calculation model

We investigated the responses of the micro fission chambers to fine the suitable position of micro fission chambers by a neutron Monte Carlo calculation using MCNP version 4b code[10]. Full sectors of the first wall, shielding blanket, some filler modules and vacuum vessel are modeled as shown in Figure 2.2-3. The input file of the MCNP code is shown in Appendix. The divertor cassettes, ports and coils are not included. Toroidal gaps besides of filler modules are modeled. However, poloidal gaps between adjacent blankets are not modeled. We use the neutron cross-section set based on JENDL 3.2[11].

The neutron source is toroidally symmetric source with 14 MeV monoenergetic energy. The source has a poloidal distribution as follows;

$$s = \left[1 - \left\{\frac{\left(R - R_p + \delta a - f(z)\right)^2}{a^2} + \frac{\left(z - Z_p\right)^2}{a^2 \kappa^2}\right\}\right]^m$$

$$f(z) = \delta a \left[1 - \frac{\left(z - Z_p\right)^2}{a^2 \kappa^2}\right]^n \qquad (2.2\text{-}1)$$

Where R_P is the major radius, a is the minor radius, Z_P is the vertical shift of the plasma center, κ is the ellipticity, δ is the triangularity and m is the power of the parabolic profile. Parameter n determines the triangular shape of the plasma. The angular emission is isotropic. The reference parameters are R_P = 6.2 m, a = 2.0 m, Z_P = 0.53 m, κ = 1.7, m = 0.8 and n = 0.5. This formula can represent the neutron source profile of ITER-FEAT. In this case, the neutron source peaking factor is represented by

$$\frac{S_n(0)}{\langle S_n \rangle} = m + 1 \qquad (2.2\text{-}2)$$

Where $S_n(o)$ and $<S_n>$ are the central and volume averaged neutron emissivity, respectively.

Energy groups in the MCNP calculation is shown in Table 2.2-1.

Table 2.2-1 Energy groups in the MCNP calculation.

Number	Upper Energy (MeV)	Lower Energy (MeV)	Lethergy width
1	1.0000E-06	5.5000E-07	5.9784E-01
2	2.1500E-06	1.0000E-06	7.6547E-01
3	4.6500E-06	2.1500E-06	7.7140E-01
4	1.0000E-05	4.6500E-06	7.6572E-01
5	2.1500E-05	1.0000E-05	7.6547E-01
6	4.6500E-05	2.1500E-05	7.7140E-01
7	1.0000E-04	4.6500E-05	7.6572E-01
8	2.1500E-04	1.0000E-04	7.6547E-01
9	4.6500E-04	2.1500E-04	7.7140E-01
10	1.0000E-03	4.6500E-04	7.6572E-01
11	2.1500E-03	1.0000E-03	7.6547E-01
12	4.6500E-03	2.1500E-03	7.7140E-01
13	1.0000E-02	4.6500E-03	7.6572E-01
14	2.1500E-02	1.0000E-02	7.6547E-01
15	4.6500E-02	2.1500E-02	7.7140E-01
16	1.0000E-01	4.6500E-02	7.6572E-01
17	1.4100E-01	1.0000E-01	3.4359E-01
18	2.0000E-01	1.4100E-01	3.4956E-01
19	2.8300E-01	2.0000E-01	3.4713E-01
20	4.0000E-01	2.8300E-01	3.4602E-01
21	5.6600E-01	4.0000E-01	3.4713E-01
22	8.0000E-01	5.6600E-01	3.4602E-01
23	1.0580E+00	8.0000E-01	2.7952E-01
24	1.4000E+00	1.0580E+00	2.8009E-01
25	1.8710E+00	1.4000E+00	2.9000E-01
26	2.5000E+00	1.8710E+00	2.8982E-01
27	3.1620E+00	2.5000E+00	2.3491E-01
28	4.0000E+00	3.1620E+00	2.3509E-01
29	4.5160E+00	4.0000E+00	1.2133E-01
30	5.0990E+00	4.5160E+00	1.2142E-01
31	5.7570E+00	5.0990E+00	1.2137E-01
32	6.5000E+00	5.7570E+00	1.2139E-01
33	7.3280E+00	6.5000E+00	1.1990E-01
34	8.2610E+00	7.3280E+00	1.1984E-01
35	9.3140E+00	8.2610E+00	1.1997E-01
36	1.0500E+01	9.3140E+00	1.1986E-01
37	1.1478E+01	1.0500E+01	8.9057E-02
38	1.2549E+01	1.1478E+01	8.9209E-02
39	1.3720E+01	1.2549E+01	8.9214E-02
40	1.5000E+01	1.3720E+01	8.9196E-02

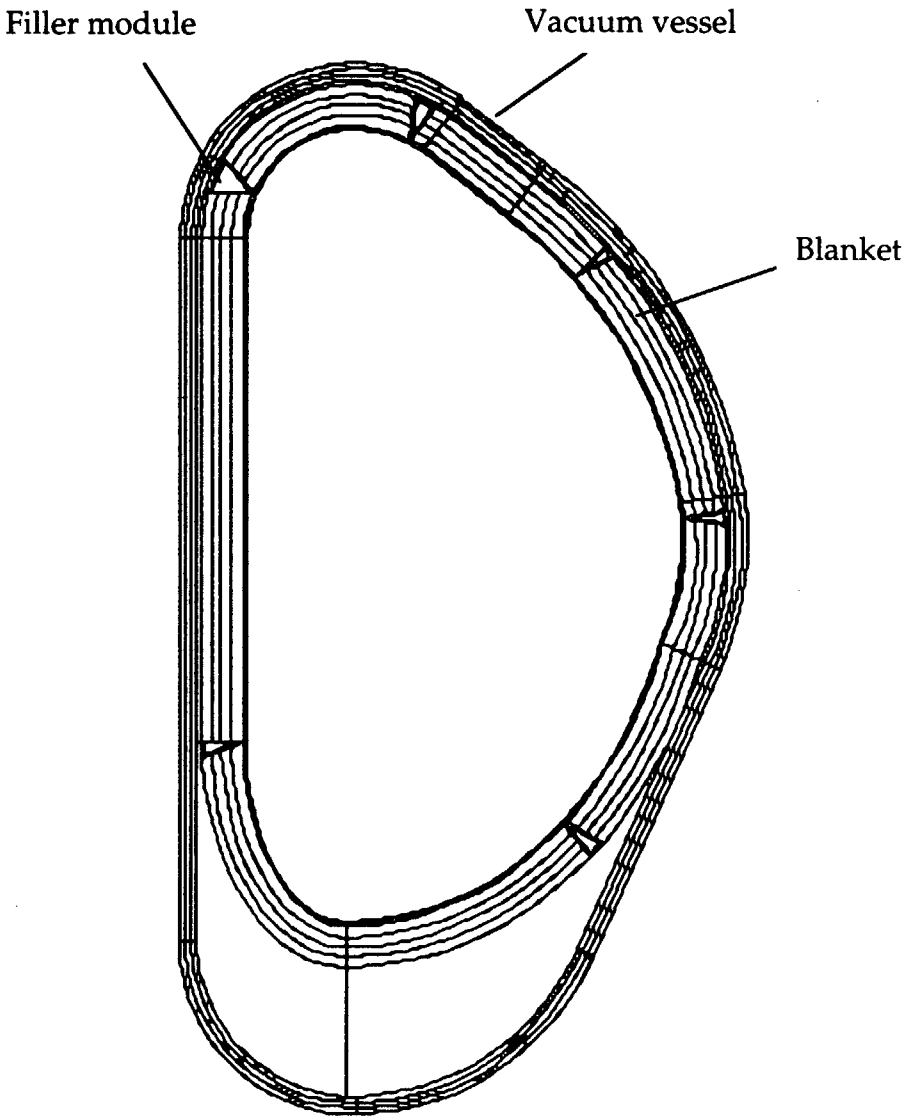

Figure 2.2-3 MCNP calculation model.

2.2.3 Neutron fluxes behind shielding blankets and at the backside of filler module.

Calculated neutron spectra behind shielding blankets and at the backside of filler module are shown in Figure 2.2-4. Here the blanket number is as shown in Fig. 2.2-5. The neutron flux at the backside of filler module is also about one order higher than that and behind the blankets, which shows that the neutron flux at the backside of the filler module is dominated by the neutron steaming along the gap between the filler module and adjacent blanket modules. So we gave up the install at the backside of filler module.

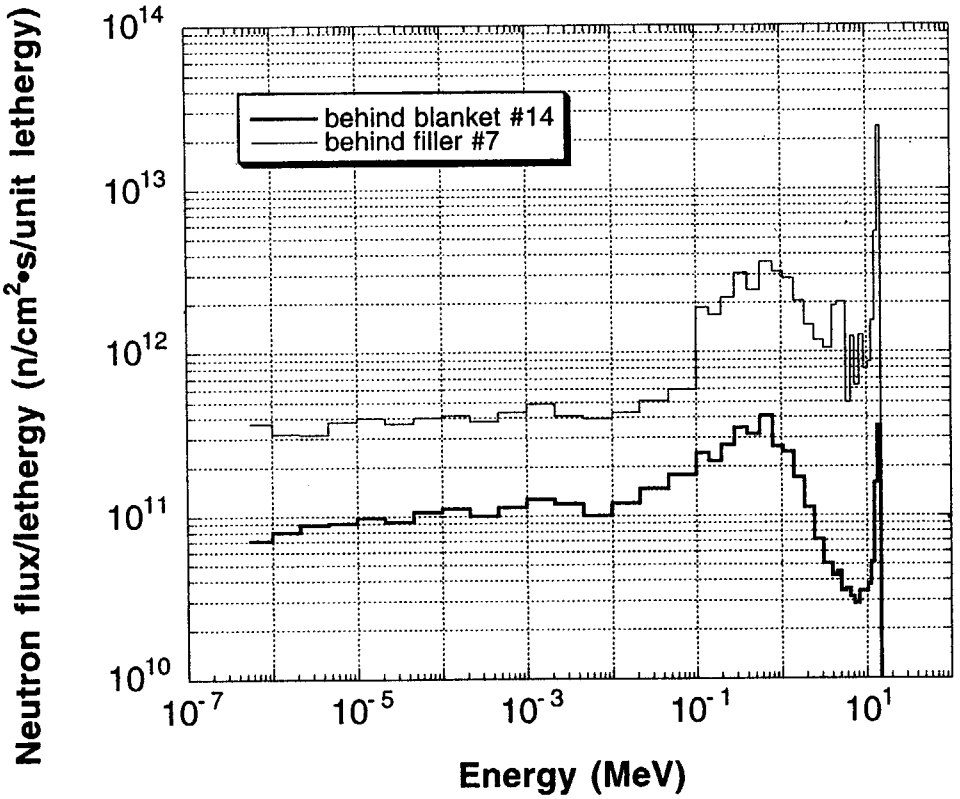

Figure 2.2-4 Calculated neutron spectra behind shielding blankets and at the backside of filler module.

2.2.4 Finding of suitable positions

The detection efficiency of a neutron detector inside the vacuum vessel seems to be affected by the change of the plasma position and the neutron source profile, because the detectors are much closer than those of ex-vessel neutron flux monitor. In ITER-FDR, we proposed 10 poloidal locations for the micro fission chambers. Here we selected the install positions, which are less sensitive to the changes in the plasma position and the neutron source profile.

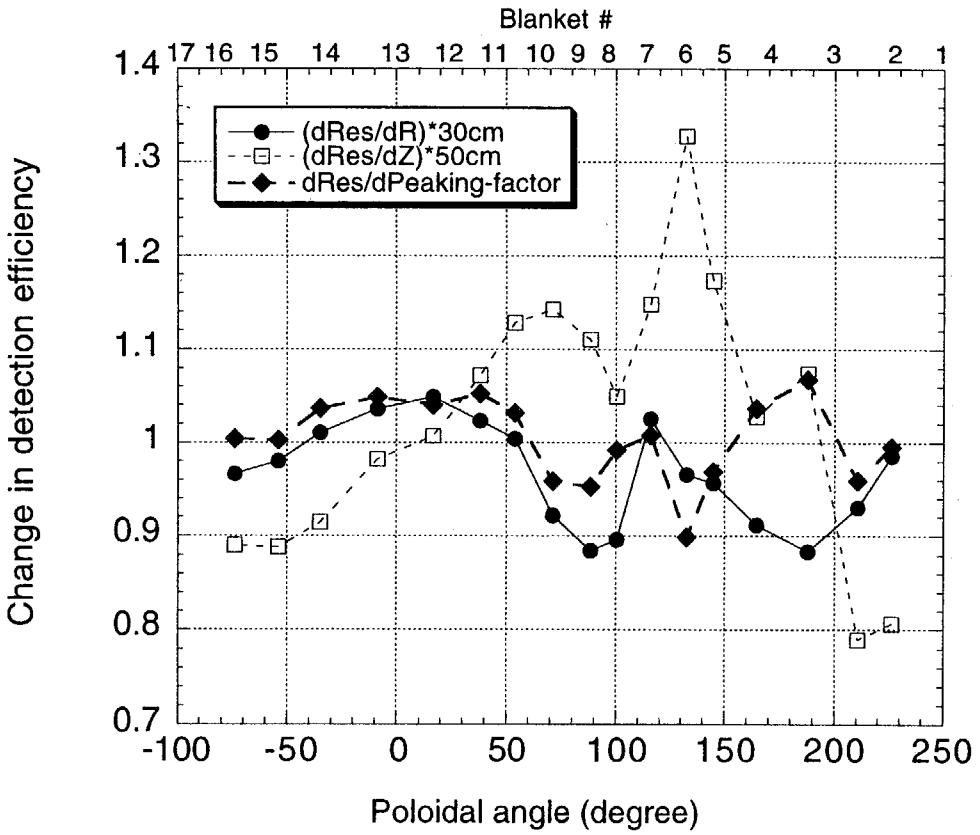

Figure 2.2-5 Changes in the detection efficiency for the changes in horizontal and vertical plasma positions, and the peaking factor of the neutron source profile

Changes in the detection efficiency for the changes in horizontal and vertical plasma positions, and the peaking factor of the neutron source profile are plotted against the poloidal angle of blankets as shown in Figure2.2-5. Positions at the blankets #11 and #16 are almost insensitive to the changes in the horizontal plasma position and the peaking factor of the neutron source profile. The changes in the vertical plasma position are opposite direction. So the averaged outputs of the micro fission chambers at #11 and #16 may be insensitive to the changes in the plasma position and the neutron source profile.

2.3 Effects of Plasma Position and Neutron Source Profile

The detection efficiency of a neutron detector inside the vacuum vessel seems to be affected by the change of the plasma position and the neutron source profile. However, we have a possibility to reject or reduce the effects by installing the detectors at several poloidal angles. We calculated the detection efficiencies and those plasma parameter dependencies of the ^{235}U micro fission chambers behind blankets #11 and #16.

2.3.1 Neutron and gamma-ray spectra

Neutron and gamma-ray spectra at the positions behind blankets #11 and #16 are shown in Figures 2.3-1 and 2.3-2. Those spectra at both positions are almost identical.

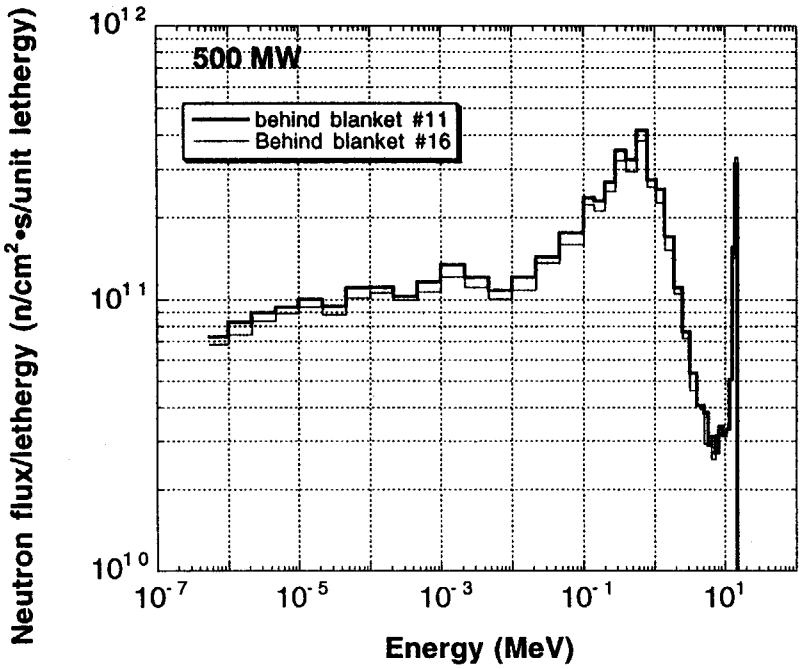

Figure 2.3-1 Neutron spectra at the positions behind blankets #11 and #16.

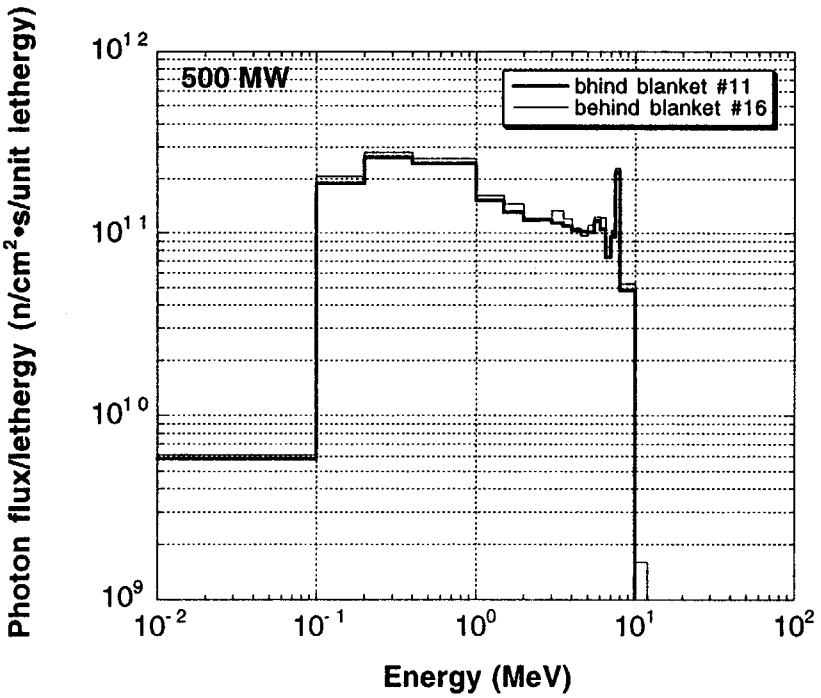

Figure 2.3-2 Gamma-ray spectra at the positions behind blankets #11 and #16.

2.3.2 Detection efficiencies for the changes in the plasma position and the neutron source profile

Dependence of the detection efficiencies for the horizontal plasma shift is shown in Figure 2.3-3. The detection efficiencies are very week functions against the horizontal plasma position.

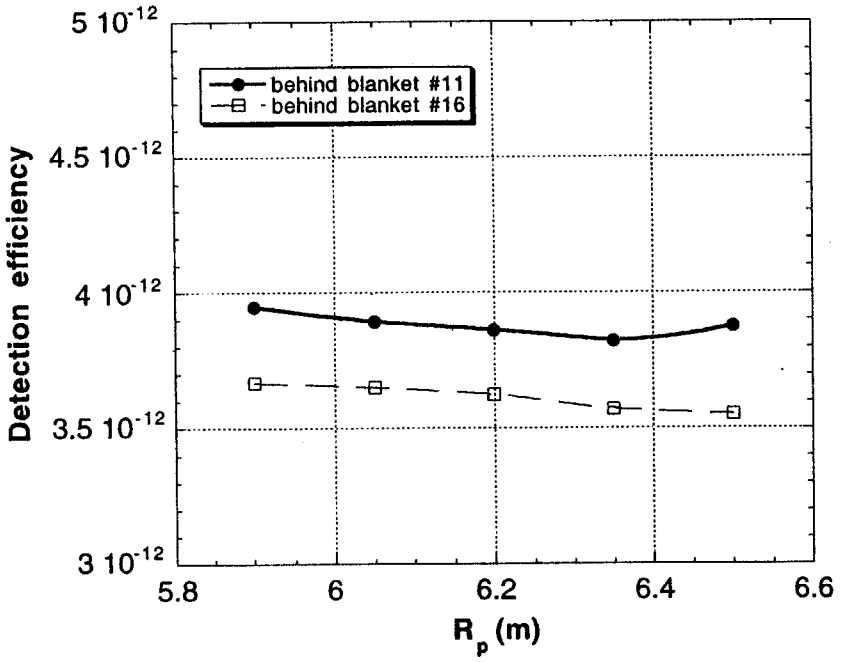

Figure 2.3-3 Dependence of the detection efficiencies for the horizontal plasma shift

Dependence of the detection efficiencies for the vertical plasma shift is shown in Figure 2.3-4. The detection efficiency at #11 increases monotonically with the vertical plasma shift. On the other hand, that at #16 decreases.

Dependence of the detection efficiencies for the changes in the peaking factor of the neutron source profile is shown in Figure 2.3-5.

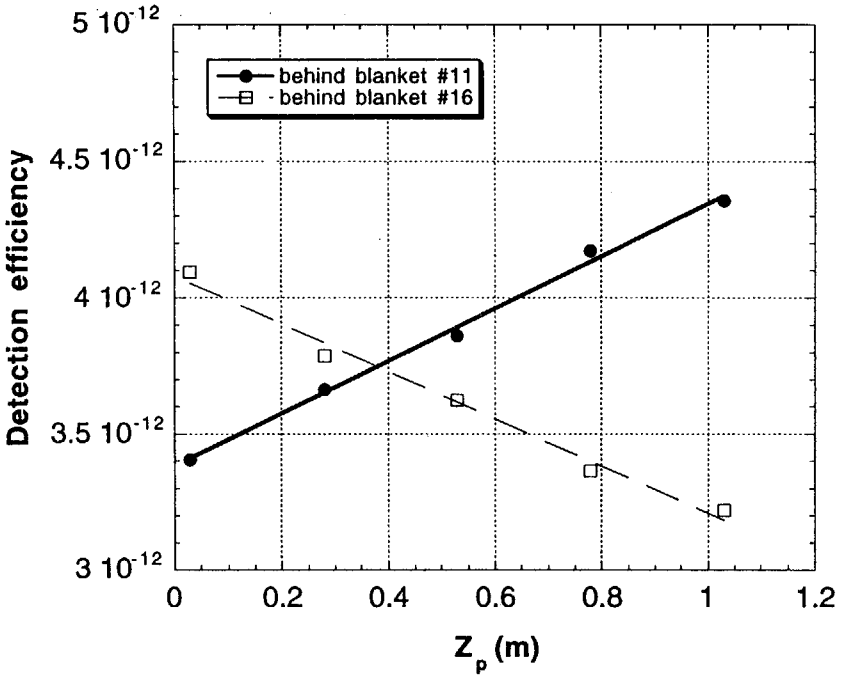

Figure 2.3-4 Dependence of the detection efficiencies for the vertical plasma shift.

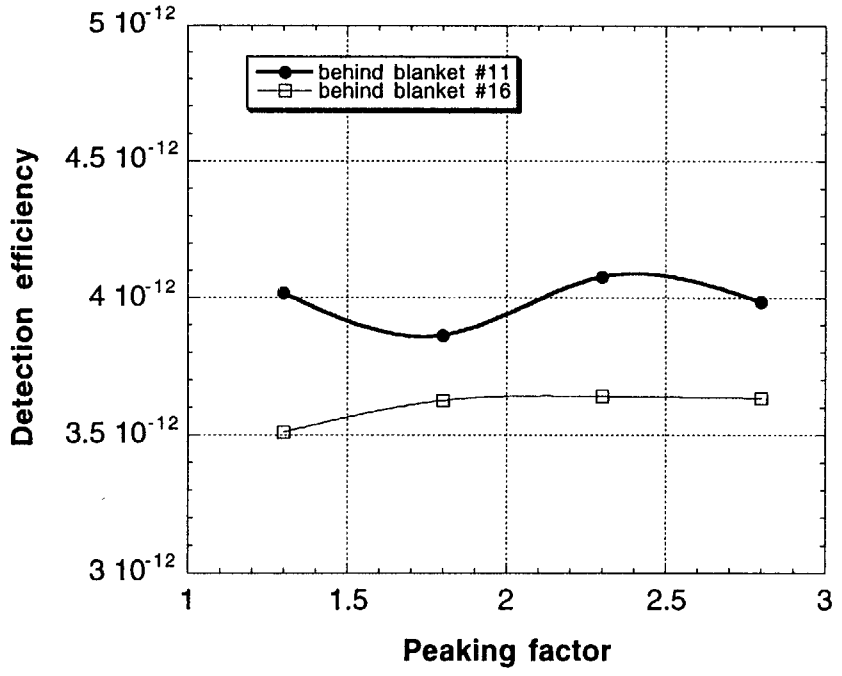

Figure 2.3-5 Dependence of the detection efficiencies for the changes in the peaking factor of the neutron source profile.

2.3.3 Effects of the plasma position and the neutron source profile on the total neutron emission rate from the micro fission chambers

The total neutron emission rate can be represented by the linear combination of the micro fission chamber counts as follows;

$$S_n = w_{11} C_{11}/\varepsilon_{11} + w_{16} C_{16}/\varepsilon_{16}$$
$$w_{11} + w_{16} = 1 \qquad (2.3\text{-}1)$$

Where S_n is the total neutron emission rate, w_i is a weigh for the linear combination, C_i is a count rate, and ε_i is detection efficiency for the reference plasma parameters. The weights w_i are determined to minimize the deviation of the total neutron emission rate.

From the calculation shown in Figures 2.3-3 - 2.3-5, following parameters were obtained;

$\varepsilon_{11} = 3.86 \times 10^{-12}$ counts/source_neutron

$\varepsilon_{16} = 3.63 \times 10^{-12}$ counts/source_neutron

$w_{11} = 0.49$

$w_{16} = 0.51$

The errors of the total neutron emission rate due to changes in the plasma parameters are shown in Figures 2.3-6 - 2.3-8. We found that the errors due to changes in the plasma parameters are less than ±3%.

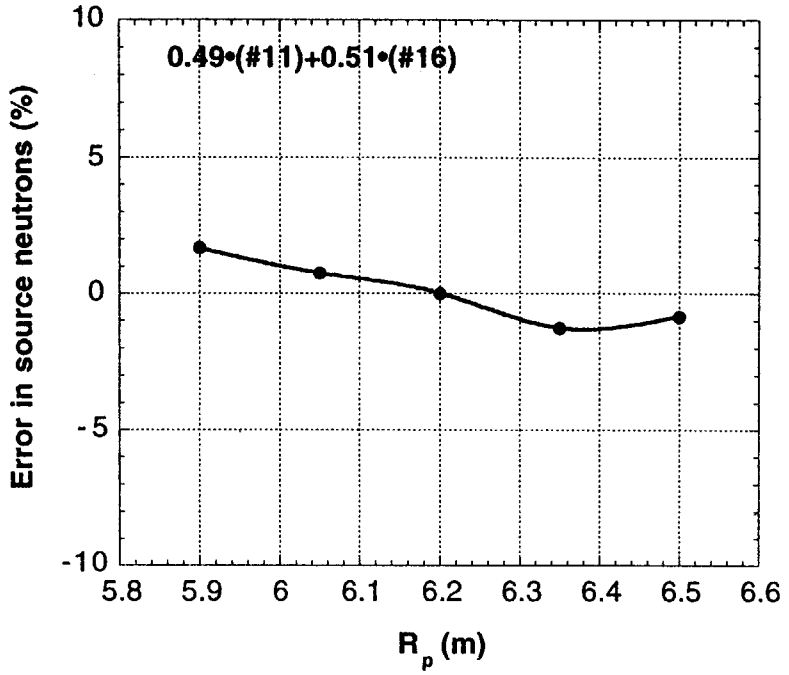

Figure 2.3-6 Errors of the total neutron emission rate for the horizontal plasma shift.

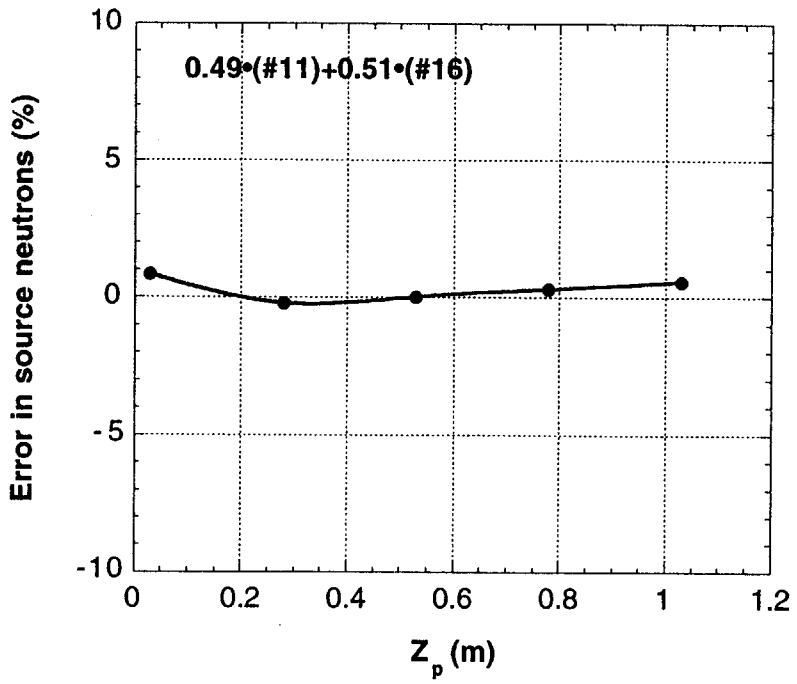

Figure 2.3-7 Errors of the total neutron emission rate for the vertical plasma shift.

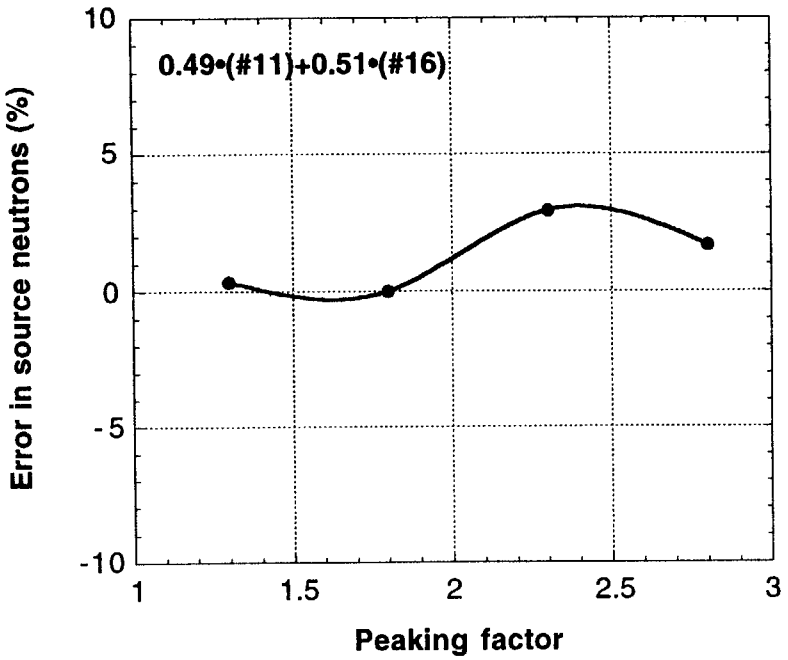

Figure 2.3-8 Errors of the total neutron emission rate for the changes in the peaking factor of the neutron source profile.

2.4 Lifetime Estimation

A lifetime of the micro fission chamber is determined by the change of the sensitivity of the chamber due to the burn-up of the fissile material. ^{235}U is burned up through mainly fission and neutron capture reactions. So the number of ^{235}U atoms, N_{235U}, is represented by following equation;

$$\frac{d}{dt}N235U(t) = -N235U(t)\phi(\sigma_{f235U} + \sigma_{C235U}) \tag{2.4-1}$$

where σ_{f235U} and σ_{C235U} are averaged fission and neutron capture cross-sections defined by

$$\sigma = \frac{\int \sigma(E)\phi(E)dE}{\int \phi(E)dE} \tag{2.4-2}$$

where $\phi(E)$ is the neutron energy spectrum at the micro fission chamber.
From equation (2.4-1),

$$\begin{aligned} N_{235U}(t) &= N_{235U}(0)Exp\{-\phi(\sigma_{f235U} + \sigma_{C235U})t\} \\ &\approx N_{235U}(0)\{1-\phi(\sigma_{f235U} + \sigma_{C235U})t\} \\ &\approx N_{235U}(0)(1-\phi\sigma_{f235U}\, t) \end{aligned} \tag{2.4-3}$$

is obtained. For the detector position behind a blanket (typically #11), the burn-up of ^{235}U atoms is dominated by the fission reaction, because the fission cross section is about 10^2 larger than the capture one. The burn-up rate of $\phi\sigma_{f235U}$ is 2.7×10^{-11} s^{-1} as shown in Table 2.4-1. The change of the sensitivity is estimated to be only 0.1 % behind blankets for the ITER life time which is equivalent to 0.5 GW•year. So we can use ^{235}U chambers without replacement in the ITER lifetime.

Table 2.4-1 Burn-up rate of U235 at the detector position behind blanket.

Energy (MeV)	Neutron flux for 500MW n/cm2·s	U-235 Fission cross-section barns (e-24 cm2)	$\phi\sigma$ s-1
1.000E-06	4.35E+10	64.688	2.815E-12
2.150E-06	6.30E+10	36.043	2.272E-12
4.650E-06	6.90E+10	16.955	1.169E-12
1.000E-05	7.16E+10	46.482	3.328E-12
2.150E-05	7.66E+10	45.366	3.474E-12
4.650E-05	7.29E+10	43.188	3.149E-12
1.000E-04	8.45E+10	34.543	2.919E-12
2.150E-04	8.48E+10	21.076	1.787E-12
4.650E-04	7.93E+10	16.454	1.305E-12
1.000E-03	8.89E+10	11.257	1.001E-12
2.150E-03	1.03E+11	7.0442	7.253E-13
4.650E-03	9.30E+10	4.7953	4.460E-13
1.000E-02	8.28E+10	3.3453	2.771E-13
2.150E-02	9.23E+10	2.4773	2.288E-13
4.650E-02	1.11E+11	2.0224	2.243E-13
1.000E-01	1.34E+11	1.7096	2.299E-13
1.410E-01	8.08E+10	1.5112	1.221E-13
2.000E-01	8.04E+10	1.3853	1.114E-13
2.830E-01	9.31E+10	1.2883	1.200E-13
4.000E-01	1.21E+11	1.2272	1.488E-13
5.660E-01	1.12E+11	1.1612	1.306E-13
8.000E-01	1.44E+11	1.1182	1.611E-13
1.058E+00	7.65E+10	1.1732	8.980E-14
1.400E+00	7.10E+10	1.2389	8.796E-14
1.871E+00	4.95E+10	1.2676	6.268E-14
2.500E+00	3.20E+10	1.2926	4.135E-14
3.162E+00	1.78E+10	1.2411	2.207E-14
4.000E+00	1.26E+10	1.1832	1.489E-14
4.516E+00	4.94E+09	1.1428	5.642E-15
5.099E+00	4.92E+09	1.0875	5.353E-15
5.757E+00	4.63E+09	1.0408	4.817E-15
6.500E+00	3.51E+09	1.1503	4.039E-15
7.328E+00	3.75E+09	1.539	5.768E-15
8.261E+00	3.25E+09	1.7649	5.735E-15
9.314E+00	4.07E+09	1.7687	7.197E-15
1.050E+01	3.76E+09	1.7381	6.536E-15
1.148E+01	2.96E+09	1.7082	5.061E-15
1.255E+01	4.50E+09	1.7598	7.920E-15
1.372E+01	1.39E+10	1.9401	2.687E-14
1.500E+01	2.78E+10	2.0941	5.818E-14
		Total	2.661E-11

2.5 Dynamic Range

Wide dynamic range of 10^7 in single fission chamber has been demonstrated in the JT-60U neutron monitor[3] with both pulse counting and Campbelling modes, which meets the ITER requirement for the neutron monitor. The linearity was calibrated using a fission reactor with output power range of 10^7 before installation on JT-60U. Because the pulse width of the fission chamber output is about 100 ns, the maximum pulse counting rate is about 10^6 counts/s due to pulse pile-up. The Campbelling mode is available for equivalent counting rate more than 10^5 counts/s. We confirmed one decade of overlap in pulse counting and Campbelling modes. From this experience, expected dynamic range of micro fission chamber with 10 mg ^{235}U is shown in Figure 2.5-1. So this system can cover the 10^7 of ITER operation range.

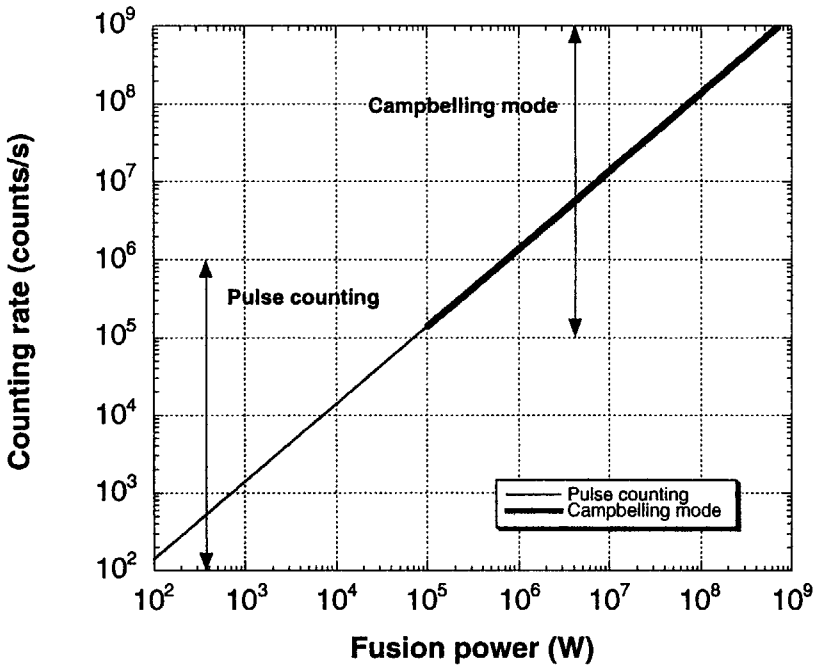

Figure 2.5-1 Dynamic range of micro fission chamber with 10 mg ^{235}U.

However, statistical error of the pulse counting is a problem for lower fusion power. Statistical error of the pulse counting is plotted against the fusion power for 1 ms and 10 ms sampling times in Fig.2.5-2. If we keep the statistical error to be less than 10%, realistic dynamic range is 100 kW – 1GW of the fusion power for 1 ms sampling time. For longer sampling time such as 10 ms at the lower fusion power, we can extend the measurement limit to 10 kW operation.

In the case of DD operation, the fusion power is estimated to be about 2 orders lower than DT operation. So the effective dynamic range of the micro fission chamber system is only 2-3 decades at the DD operation. The installation space is too tight to increase the amount of fissile material in the micro fission chamber which needs bigger size. We had better use a high sensitive detector for the low power DT operation or DD operation. The high sensitive detector will be installed in the port plug and is designed as a neutron flux monitor system (WBS 5.5B. 04).

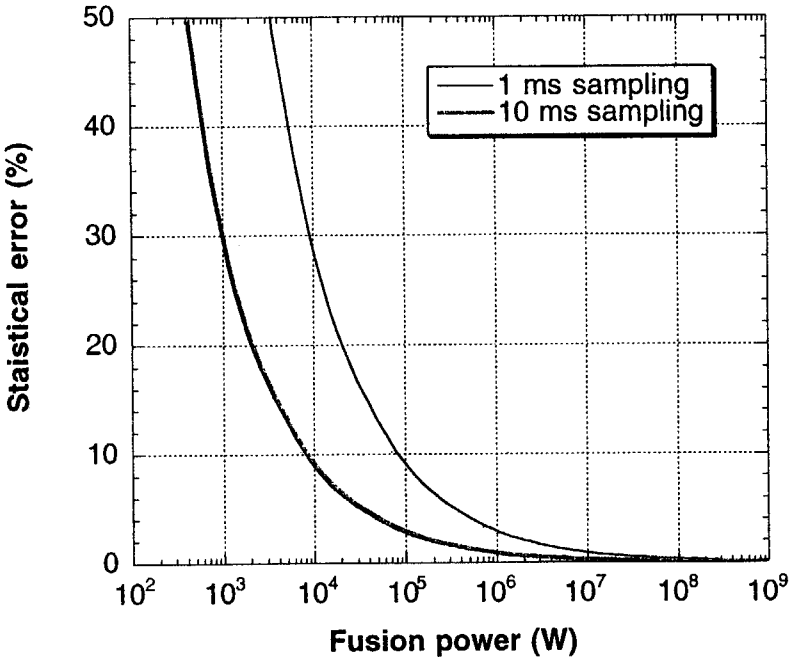

Figure 2.5-2 Statistical error of the pulse counting plotted against the fusion power for 1 ms and 10 ms sampling times.

2.6 Gamma-ray Effect

This micro fission chamber can be operated in the pulse counting and the Campbelling modes. In the pulse counting mode, current pulse generated by the fission fragments or gamma reaction in the ionizing gas is measured. The fission reaction releases ~170 MeV as the kinetic energy of fission fragments. One fragment goes into the ionization gas and another goes into electrode wall. Average energy deposited in the ionization gas is 70 – 100 MeV, on the other hand gamma energy is less than 10 MeV (see Fig.2.3-2). So we can eliminate the gamma pulses by conventional pulse discrimination technique. The Campbell mode is less sensitive to gamma-rays and the gamma-ray effect is negligible. Based on the gamma-ray irradiation test with a dose rate of ~2MR/h carried out as the R&D task T493, the gamma-ray effects are summarized in Table 2.6-1. From this table, we do not need gamma-ray compensation detector which is same size detector without fissile material. However, we decided to employ the dummy detector not only for the gamma-ray compensation but also identification of noise events and radiation induced events such as RIEMF (Radiation Induced Electrical Motive Force).

Table 2.6-1 Outputs of the micro fission chamber by neutrons and gamma-rays at 500 MW.

Neutron Flux behind the blanket	2.3×10^{16} n/ $m^2 \cdot s$
Gamma dose rate behind the blanket	2.4×10^{6} R/h
Campbelling mode (A^2/Hz)	
Neutrons	5.9×10^{-17}
Gammas	1.9×10^{-22}
S/N ratio (Neutrons/Gammas)	3.1×10^{5}
Current mode (A)	
Neutrons	6.7×10^{-4}
Gamma-rays	3.7×10^{-6}
S/N ratio (Neutrons/Gammas)	1.8×10^{2}

2.7 Magnetic Field Effect

The effect of the strong magnetic field on the fission chamber is another problem. In the fission chamber, we measure the electron induce current from ionization by fission fragments. So we calculated the electron drift orbit in the magnetic field. The electron drift velocity **u** is represented by

$$\mathbf{u} = \frac{\mu_e}{1 + \omega_c^2/\nu^2}\left[E + \frac{\mathbf{E}\times\mathbf{B}}{B}\frac{\omega_c}{\nu} + \frac{(\mathbf{E}\cdot\mathbf{B})}{B^2}\frac{\omega_c^2}{\nu^2}\right] \qquad (2.7\text{-}1)$$

where m_e is the electron mobility, n is the collision frequency of the electron to neutral atoms, and w_c is the electron cyclotron frequency in the magnetic field **B**. If we assume **E** = (E_x, 0, 0) and **B** = (0, 0, B_z),

$$\mathbf{u} = \left(\frac{\mu_e E_x}{1 + \omega_c^2/\nu^2}, \frac{\mu_e E_x}{1 + \omega_c^2/\nu^2}\frac{\omega_c}{\nu}, 0\right) \qquad (2.7\text{-}2)$$

An angle between **u** and **E**, Lorentz angle α, is represented by $\tan\alpha = \omega_c/n$. In the case of the micro fission chamber with 14.6 atm Argon gas, applied voltage of 200 V to 0.5 mm electrode gap, in the magnetic field of 5.7 T, the mobility without magnetic field is $u_0 \approx 3 \times 10^3$ m/s. the Lorentz angle is evaluated as, $\tan\alpha \approx 0.04 << 1$.

Thus the magnetic effect on the electron drift velocity is to be negligible. However, we do not have experience of a fission chamber using in high magnetic field such as 5.3T. We should confirm the magnetic effects on the fission chamber experimentally.

2.8 Nuclear Heating

Nuclear heating of the detector is an important issue for the in-vessel diagnostics. Active water cooling of the detector is rather difficult due to the tight space between the blanket modules and back plate. The nuclear heating of the micro fission chamber is estimated to be 0.1 - 0.2 W/cc at the detector position behind the blanket module. The micro fission chamber can be operated up to 300 °C, so that it seems possible to cool it by thermal contact with the vacuum vessel which is cooled by water.

2.9 Calibration

Absolute calibration for the total neutron yield is the most critical issue in the design of the neutron monitor. In the present tokamaks, neutron monitors are calibrated by moving neutron source such as ^{252}Cf radioactive source or the DT neutron generator. In ITER, *in-situ* calibration by moving the DT neutron generator remotely inside the vacuum vessel should be performed.

We simulated the *in-situ* calibration by MCNP calculation, where a point source of 14 MeV neutrons is moving on the plasma axis with R = 6.2 m and Z=0.53 m as shown in Fig. 2.9-1. The modeling of the ITER machine is same as in Fig.2.2-3. The detector position is behind the blanket #11.

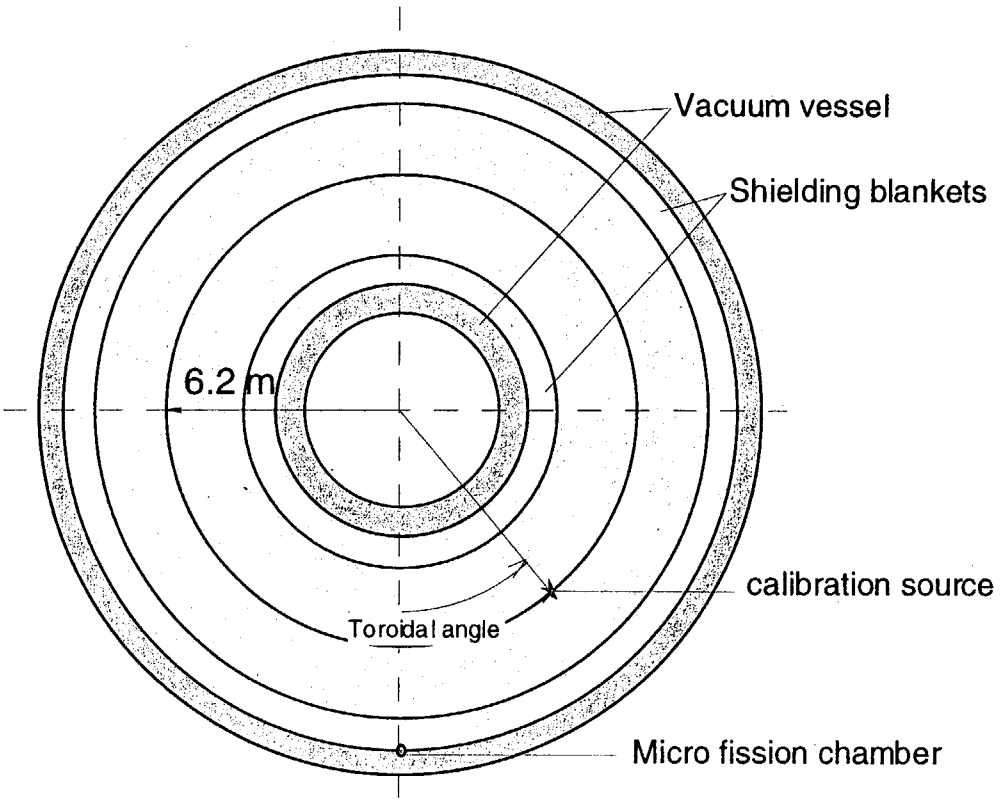

Figure 2.9-1 Calculation model of the *in-situ* calibration. A point source of 14 MeV neutrons is moving on the plasma axis with R = 6.2 m and Z=0.53 m.

Figure 2.9-2 shows the detection efficiency of the detector behind the blanket #11 for the point source on the plasma axis with R = 6.2 m plotted against the toroidal angle of the source. The sharp drop of the efficiency is observed at ±100 degree, which shows that the source goes into the shadow of the inboard blanket.

A compact DT neutron generator with emission rate of ~10^{11} neutrons/s has been developed by Russian home team, which can be installed on the remote handling apparatus and can move inside the vacuum vessel. If we use the DT neutron generator with emission rate of 1×10^{11} neutrons/s, a count rate higher than 1 count/s can be expected in the range of toroidal angle ±25 degree. Also a count rate higher than 0.1 count/s can be expected for ±100 degree.

Relative integrated efficiency is defined by,

$$\frac{\int_0^{\phi} \varepsilon(\phi) d\phi}{\int_0^{\pi} \varepsilon(\phi) d\phi} \qquad (2.9\text{-}1)$$

where $\varepsilon(\phi)$ is a detection efficiency for a point neutron source on the plasma axis with R = 6.2 m at the toroidal angle of ϕ. The relative integrated efficiency is plotted against the toroidal angle as shown in Fig.2.9-3. In this calibration, the detection efficiency for the toroidal neutron source in derived from the integration of the detection efficiencies for a point neutron source. If we scan the point source in the range of toroidal angle ±100 degree, we can obtain the detection efficiency for the toroidal neutron source with an accuracy higher than 95%. Example of the calibration procedure is shown in Table 2.9-1. In this MCNP calculation, the modeling is toroidally symmetric against the micro fission chamber, however, real ITER-FEAT machine is not symmetric. Therefore, we have to scan both toroidal direction. If we scan the point source each 10 degree in the range of toroidal angle ±100 degree, we need three days for the calibration, where the time for moving source should be taken into account.

In this calibration simulation, a point neutron source is scanned only on the plasma axis. On the real calibration experiment at TFTR, a point neutron source was scanned not only on the plasma axis but also several off-axis direction. But it takes much time. Here we discuss the difference of the detection efficiency derived from the point efficiency and that

for the distributed source with a parabolic distribution profile in a poloidal cross-section as shown in Table 2.9-2. The detection efficiency from the point source calibration agreed those for the distributed source within 5%.

In this design, micro fission chambers are operated mainly in Campbelling mode with wide dynamic range. Here, the linearity calibration of the Campbelling output is necessary before the installation. As carried out in JT-60U, the linearity calibration using a fission reactor is proposed for those micro fission chambers.

By those calibrations, the micro fission chamber system can meet the required 10% accuracy goals of the fusion power measurement for the ITER fusion power monitor.

Table 2.9-1 Procedure of the point source calibration.

Poroidal Angle degree	Detction efficiency	Accumulation time sec	Counts	Statistical error	Relative error %
-100	1.462E-12	18000	2.631E+03	51.3	1.9
-90	1.589E-12	18000	2.859E+03	53.5	1.9
-80	1.772E-12	14400	2.552E+03	50.5	2.0
-70	2.181E-12	14400	3.141E+03	56.0	1.8
-60	2.506E-12	10800	2.706E+03	52.0	1.9
-50	3.302E-12	10800	3.567E+03	59.7	1.7
-40	4.480E-12	7200	3.225E+03	56.8	1.8
-30	6.854E-12	7200	4.935E+03	70.2	1.4
-20	1.237E-11	3600	4.454E+03	66.7	1.5
-10	2.225E-11	3600	8.010E+03	89.5	1.1
0	2.837E-11	3600	1.021E+04	101.1	1.0
10	2.225E-11	3600	8.010E+03	89.5	1.1
20	1.237E-11	3600	4.454E+03	66.7	1.5
30	6.854E-12	7200	4.935E+03	70.2	1.4
40	4.480E-12	7200	3.225E+03	56.8	1.8
50	3.302E-12	10800	3.567E+03	59.7	1.7
60	2.506E-12	10800	2.706E+03	52.0	1.9
70	2.181E-12	14400	3.141E+03	56.0	1.8
80	1.772E-12	14400	2.552E+03	50.5	2.0
90	1.589E-12	18000	2.859E+03	53.5	1.9
100	1.462E-12	18000	2.631E+03	51.3	1.9
	total (hour)	61			

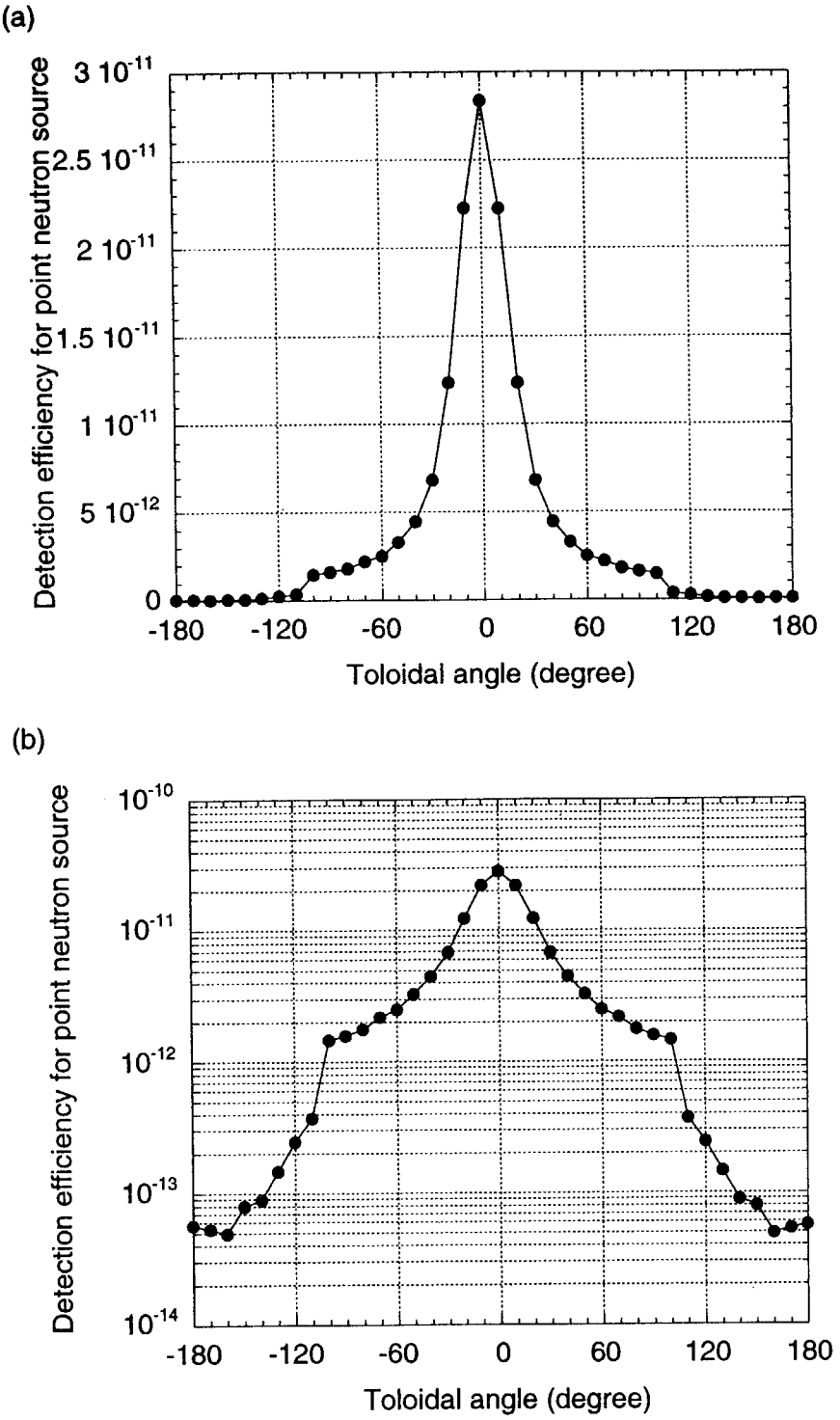

Figure 2.9-2 Detection efficiency of the detector behind the blanket #11 for the point source on the plasma axis with R = 6.2 m plotted against the toroidal angle of the source. (a) is linear plot and (b) is log plot.

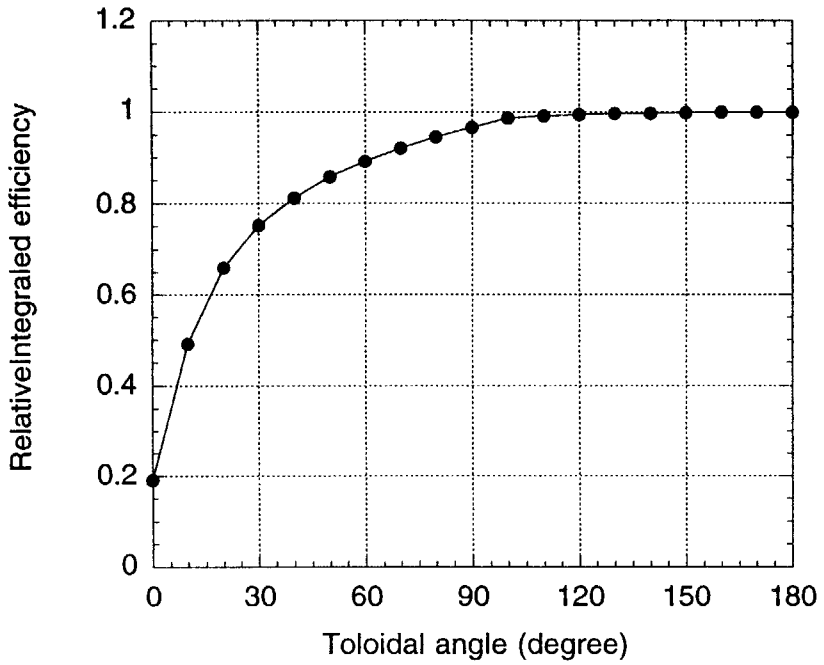

Figure 2.9-3 Relative integrated efficiency is plotted against the toroidal angle.

Table 2.9-2 Comparison of the detection efficiency derived from the point efficiency and those for the distributed source with a parabolic distribution profile in a poloidal cross-section.

	Peaking factor	Detection efficiency	Error
from point source calibration		4.11E-12	1.4%
for distributed source	1.3	4.02E-12	1.1%
	1.8	3.86E-12	1.1%
	2.3	4.08E-12	1.1%
	2.8	3.98E-12	1.1%

3. DETAILED SYSTEM DESCRIPTION

3.1 General Equipment Arrangement

The proposed arrangement of micro fission chambers on ITER is shown in Figures 3.1-1 - 3.1-3. A set of ^{235}U micro fission chamber and "blank" detector which is a fissile material free detector with same dimension as the micro fission chamber to identify noise issues such as from gamma-rays are installed behind blankets #11 and #16 in a toroidal location. We propose two toroidal locations for the redundancy.

Pre-amplifier should be located as near as possible to the fission chambers from the noise prevention point of view. Therefore, pre-amplifiers will be installed just outside of the cryostat. Integrated amplifiers and power supplies will be installed in the pit outside of the biological shield.

3.2 Micro Fission Chamber Unit

A micro fission chamber with ^{235}U and a dummy chamber are mounted in a same sheath as shown in Fig. 3.2-1. The micro fission chamber is covered with a thermal neutron shield with 1-mm thick cadmium. Both chambers are insulated electrically by a ceramics insulator. This micro fission chamber unit will be welded to the vacuum vessel directly.

3.3 Installation of Micro Fission Chambers on Vacuum Vessel

Figure 3.3-1 shows the isometric view of the micro fission chambers on the vacuum vessel. The micro fission chamber unit is located behind a blanket module as shown in Fig. 3.3-2. The sheath will be welded to the vacuum vessel which is cooled by water coolant, and through the heat conduction (see Figure 3.3-3). The outer sheath of the detector is electrically connected to the socket. However, the housing of the detector is maintained at the same ground level as the pre-amplifier. The output signal is transferred via the same MI cable as the high voltage supply. The cables are routed through diagnostic cable conduits.

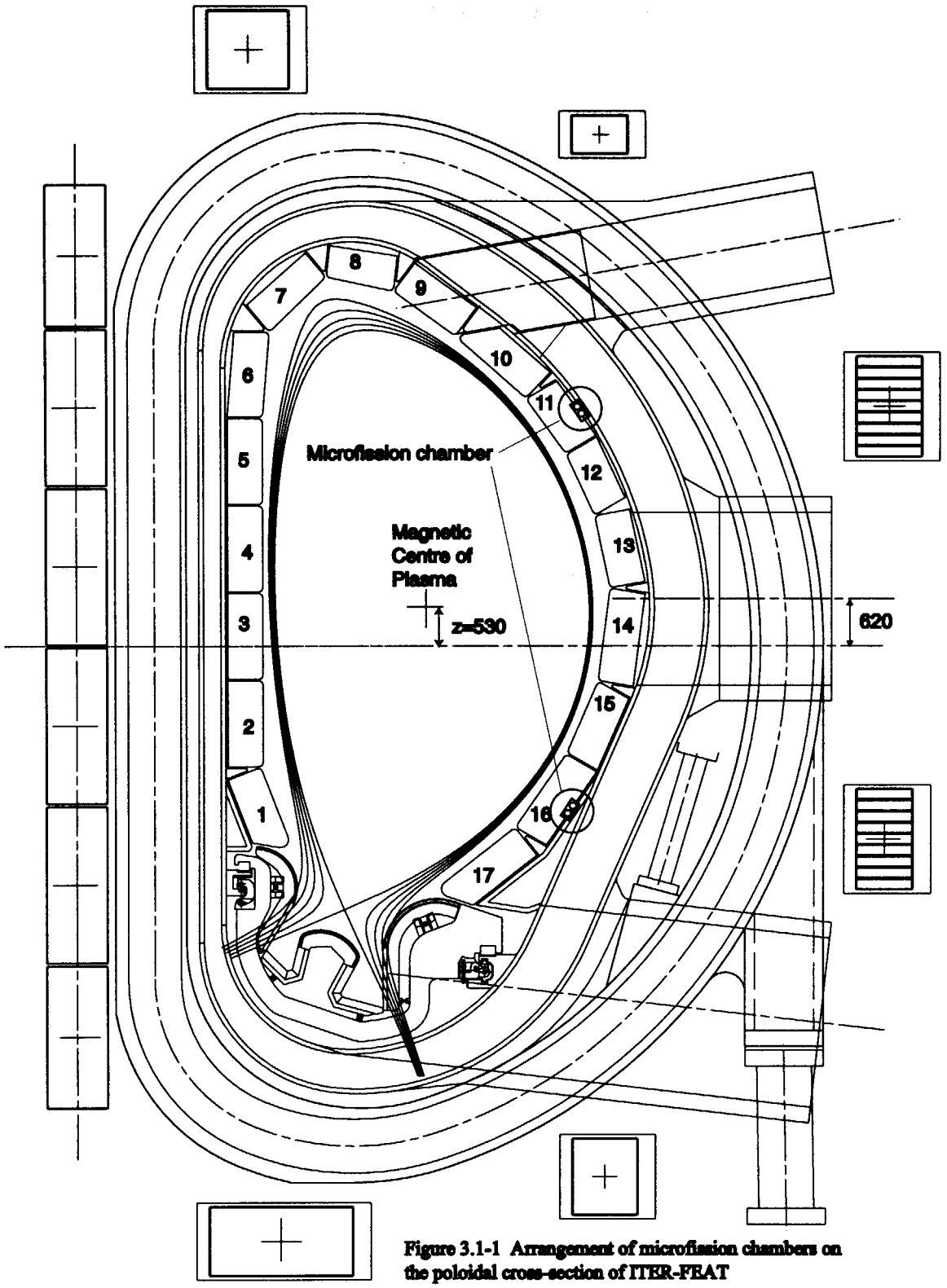

Figure 3.1-1 Arrangement of microfission chambers on the poloidal cross-section of ITER-FEAT

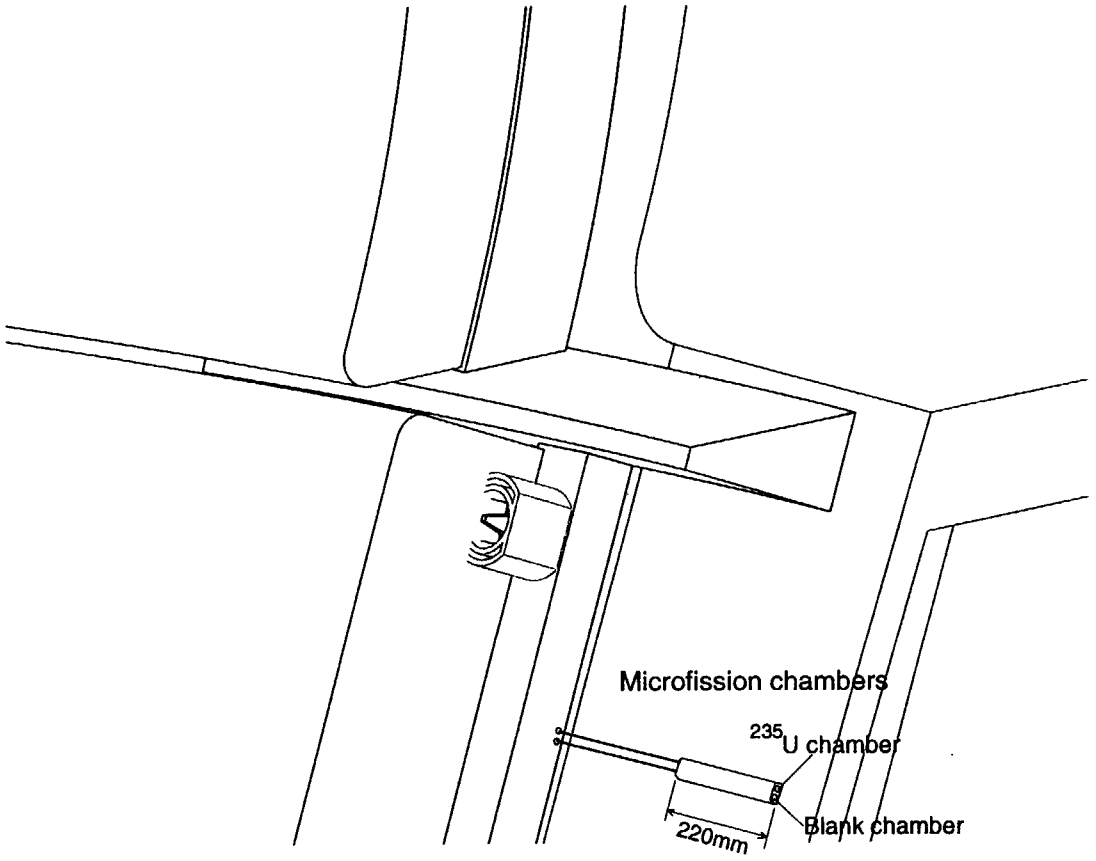

Figure 3.1-2 Concept of microfission chamber installation on the surface of the vacuum vessel

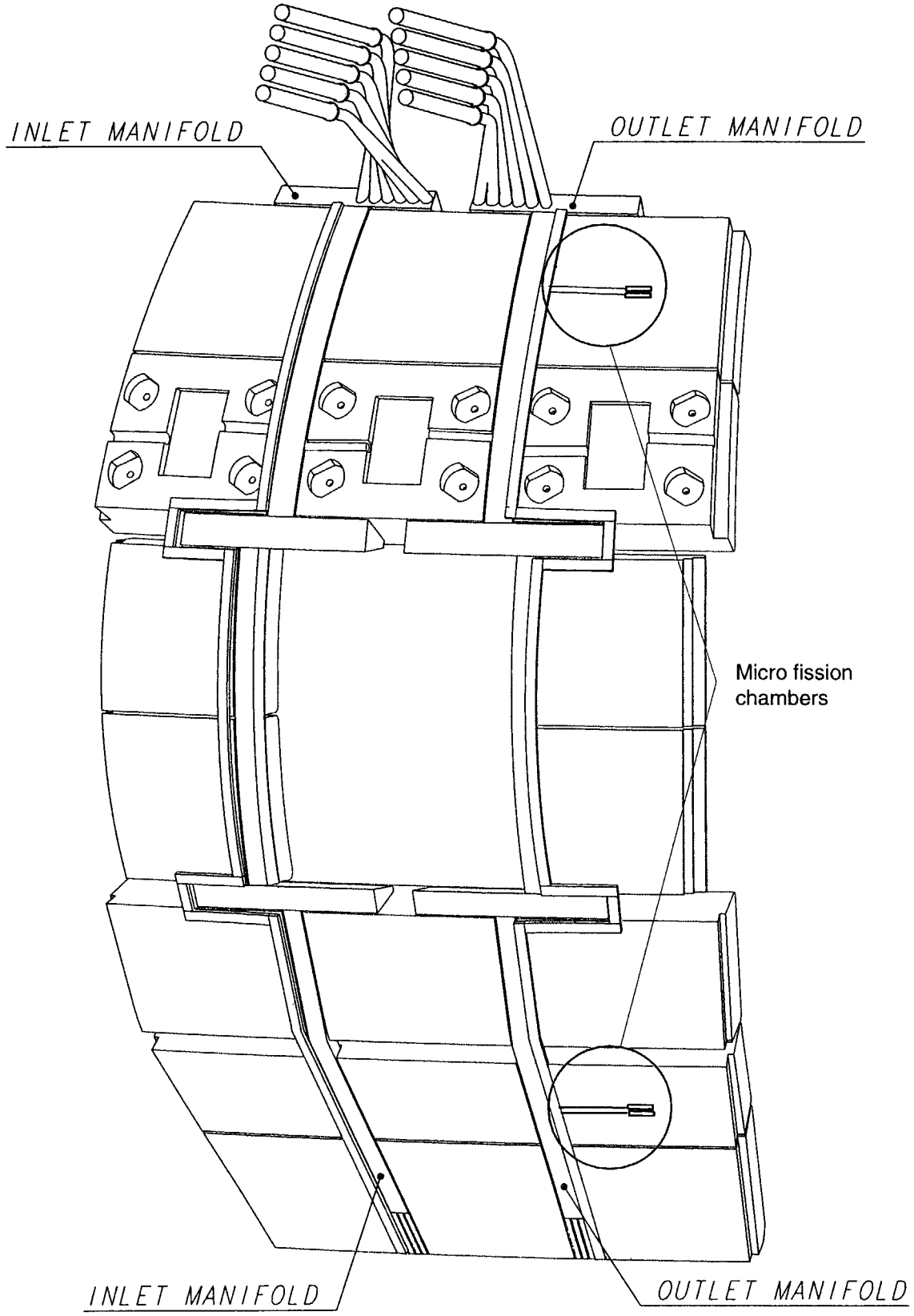

Figure 3.1-3 Arrangement of micro fission chambers.

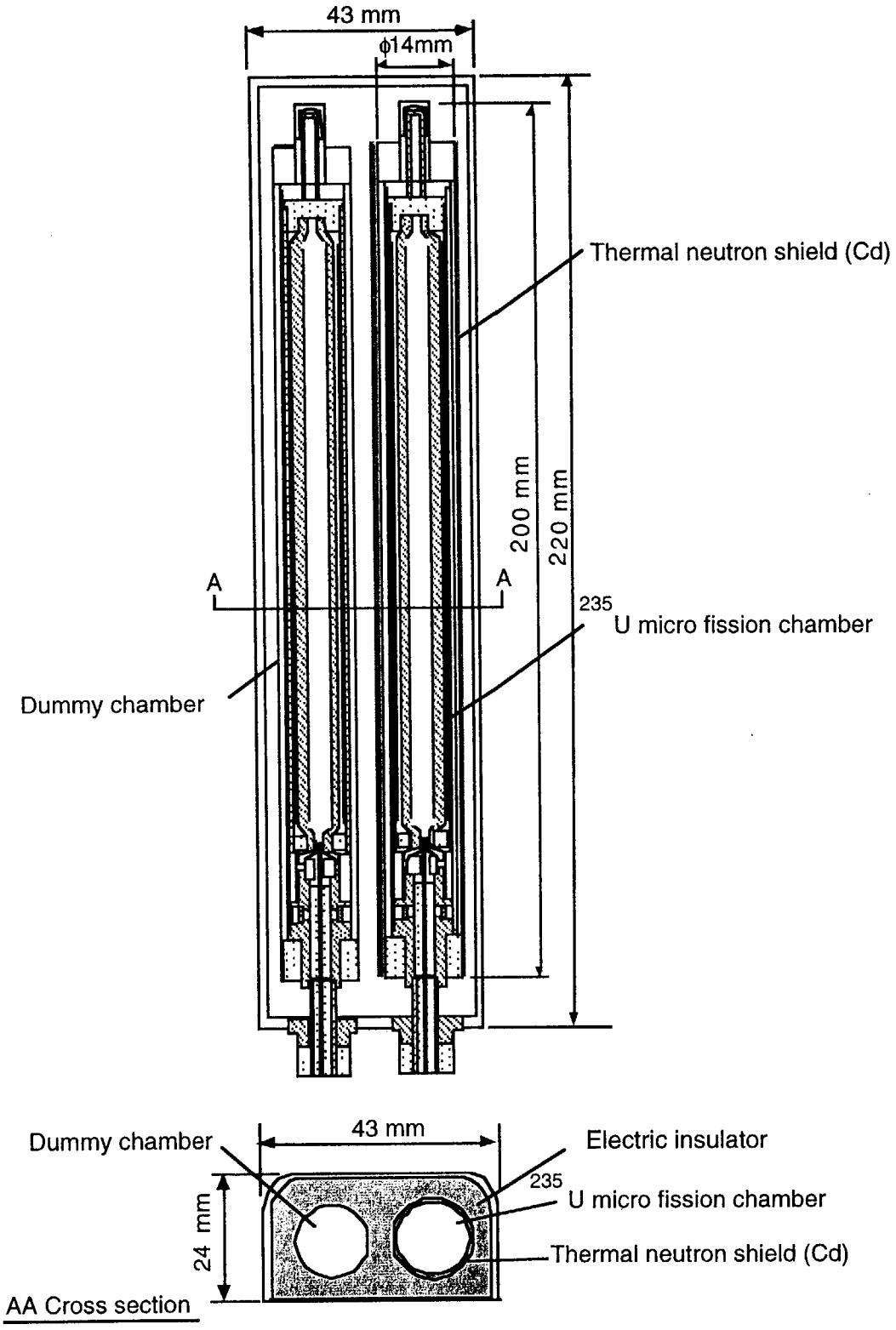

Figure 3.2-1 Schematics of micro fission chamber unit.

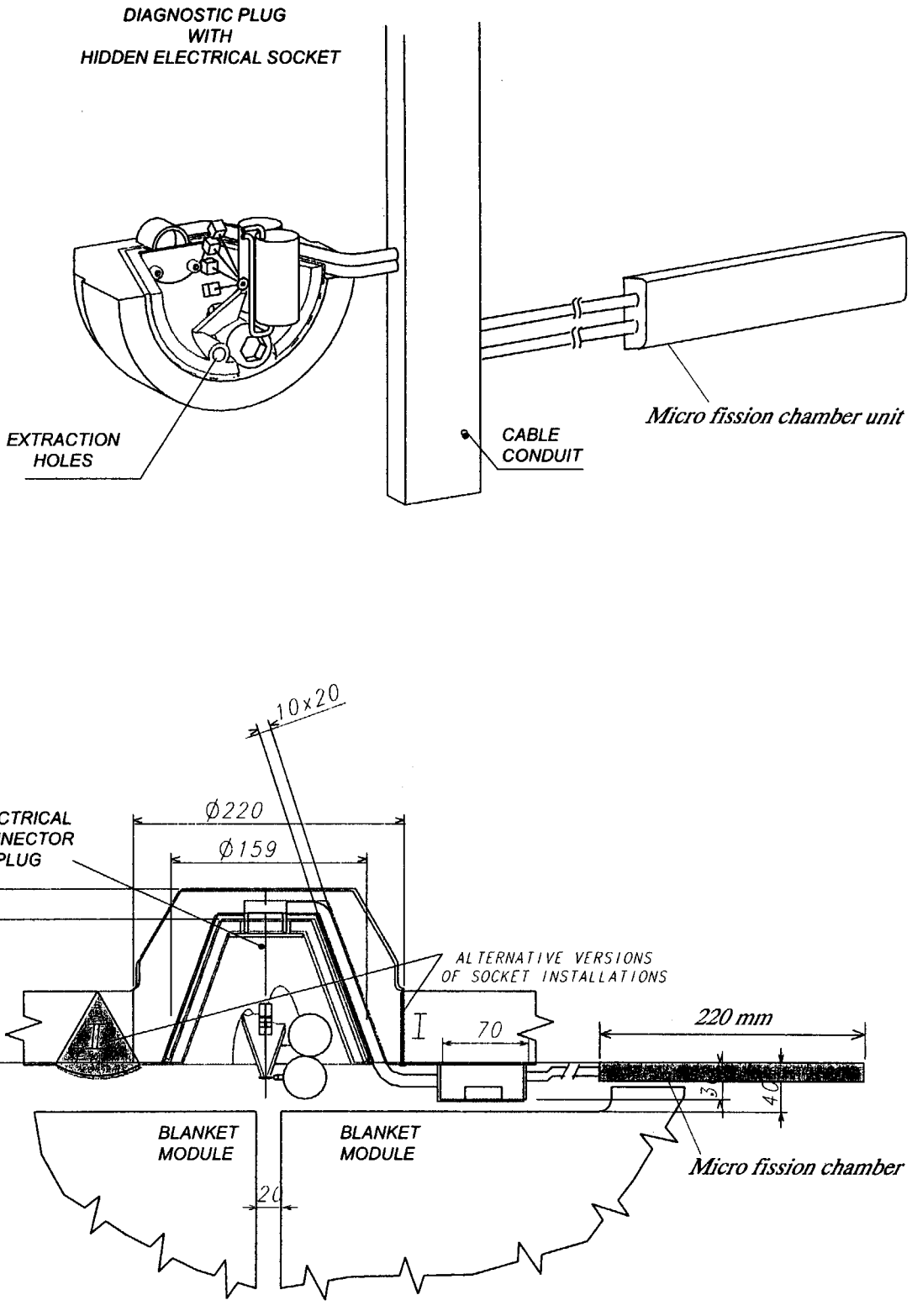

Figure 3.3-1 Isometric view of the micro fission chambers on the vacuum vessel.

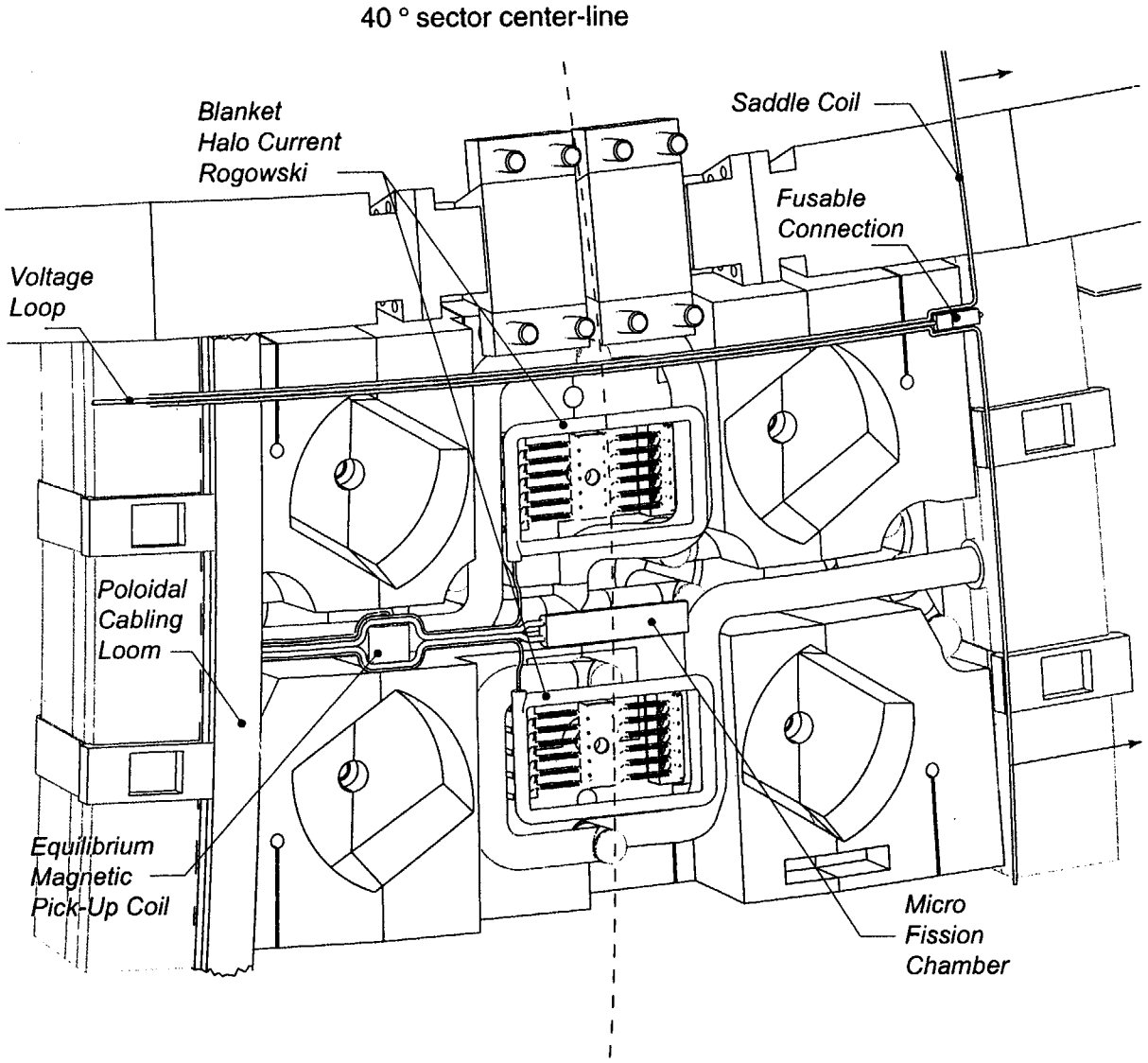

Diagnostics attached to the Vacuum Vessel at Blanket Module 11
(VV not shown)

Figure 3.3-2 Isometric view of the micro fission chambers behind the blanket module.

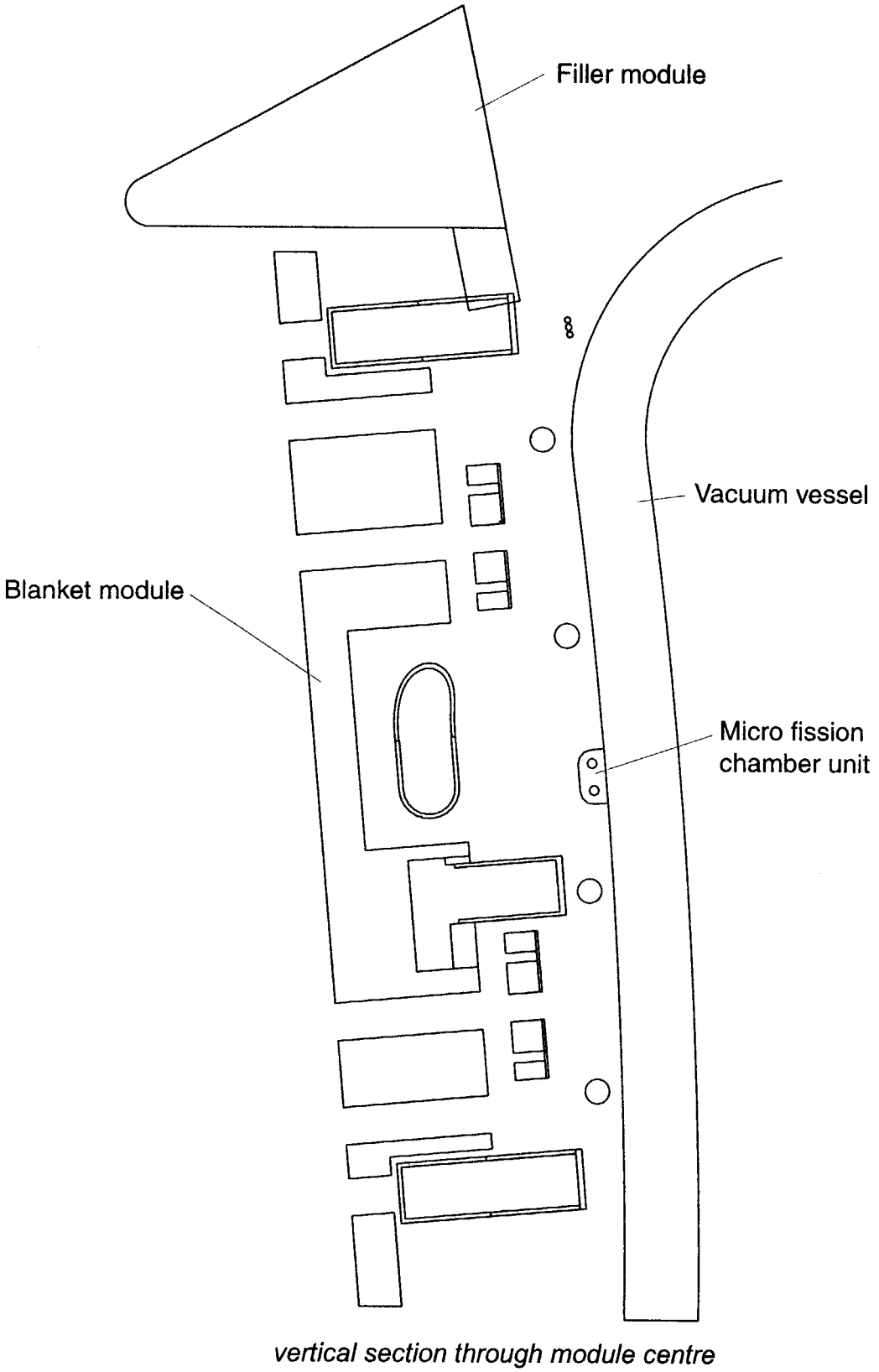

Figure 3.3-3 Cross section of the blanket module and the vacuum vessel showing the location of the micro fission chamber unit. Only the back part of the blanket is shown.

3.4 Data Acquisition and Control

A block diagram of the electronics and data acquisition equipment is shown in Fig.3.4-1. Detectors will require high voltage power supplies, preamplifiers, amplifiers, pulse counting circuitry, Campbelling amplifiers, digital equipment, etc. Preamplifiers should be installed near the detectors. Considering the radiation condition, the location in the pit near the biological shield is desirable. The integrated amplifier designed for the JT-60U neutron flux monitor consisting of a high voltage power supply, pulse amplifier, and Campbelling amplifier is preferable. The Campbelling amplifier has three different amplitude output. Typically, the relative gains are 1, 10^2 and 10^4 to get a wide dynamic range.

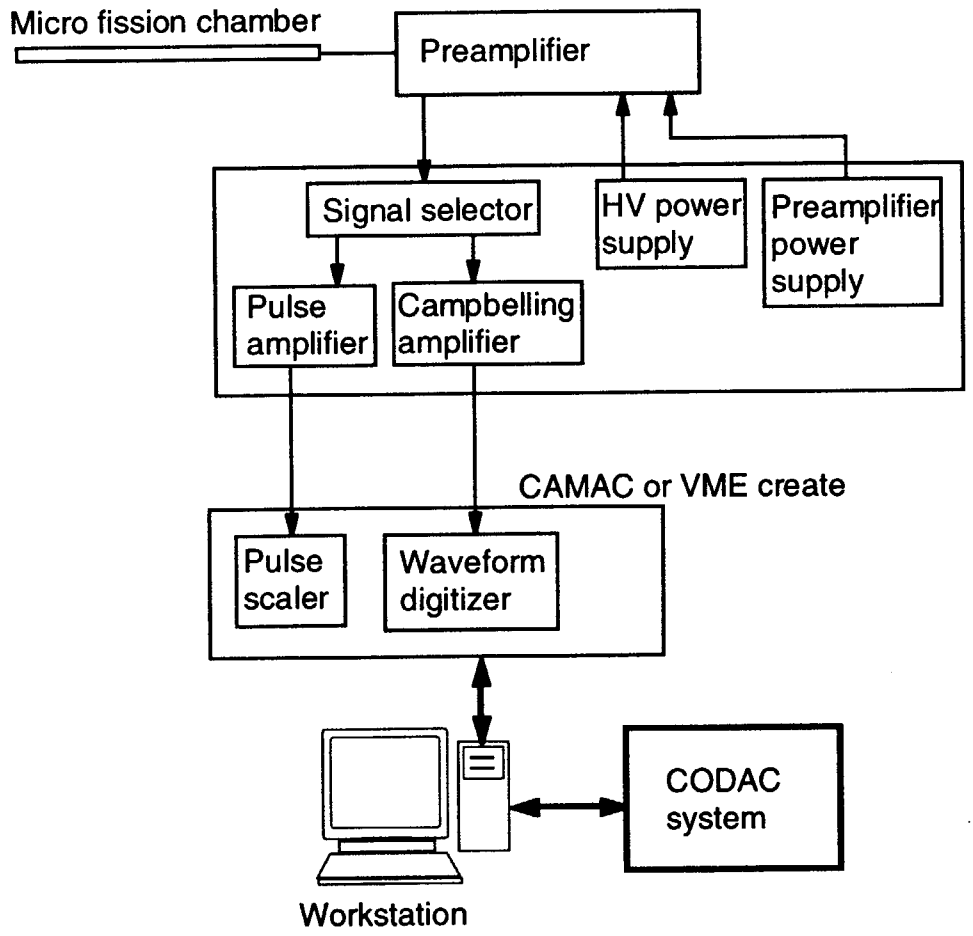

Figure 3.4-1 Block diagram of the electronics and data acquisition equipment.

The policy of the data acquisition for all diagnostics has not been established yet. We estimated the data amount of the micro fission chamber system assuming that we will measure with constant sampling time for whole discharge as shown in Table 3.4-1.

Table 3.4-1 Data amount of the micro fission chamber system.

	Number of Channels	Sampling time	Inductive operation 400 s	Hybrid operation 1000 s	Non-inductive operation 3000 s
Pulse counting	8 ch	1 ms	6.4 MB	16 MB	48 MB
Campbelling mode	8 ch × 3 gain	1 ms	38.4 MB	96 MB	288 MB
Total			44.8 MB	112 MB	336 MB

3.5 Calibration Hardware

As discussed in Section 2.9, *in-situ* calibration will be required to get the detection efficiencies for the total neutron yield or the fusion power. An essential element of such calibrations is an intense, robust, yet compact DT neutron generator. The generator should produce 14 MeV neutrons at an average rate of $\sim 10^{11}$ n/s, and be sufficiently compact and portable to allow operation inside the ITER vacuum vessel during initial system calibration and extended maintenance periods, using standard remote handling equipment, for *in situ* mapping of detector response. Of course this calibration hardware can be shared with the neutron flux monitor installed outside the vacuum vessel. So far, a neutron generator which has been developed in Russian home team is one of the candidate [12].

3.6 Component List

List of components is summarized in Table 3.6-1.

Table 3.6-1 List of components

Component	Quantity	Size (mm)	weight (kg)
^{235}U Micro Fission Chamber	4	ϕ20 × 220	1.0
"Blank" detector	4	ϕ20× 220	1.0
MI Cable	8	ϕ8	TBD
Preamplifier	8	300× 190 × 120	4
Preamplifier Box	2	600× 600 × 200	120
Integrated Amplifier	8	480× 180 × 400	10
CAMAC or VME create	2	300× 190× 120	20
ADC Module	3	222× 48× 305	2.0
Scalar Module	1	222× 16× 305	1.0
Workstation	1	TBD	TBD
Other Digital Modules	TBD	TBD	TBD
Neutron generator	1	TBD	TBD

4. OPERATION STATE DESCRIPTION

4.1 Commissioning State

All equipment should be installed in the commissioning stage of ITER. ITER has not commenced operation. All electronic equipment is accessible for testing.

4.2 Calibration State

Micro fission chambers are installed and operational. ITER has not commenced operation, and the vacuum vessel is open for in-vessel activities. Neutron generator and transport apparatus are temporarily installed inside ITER vacuum vessel before initial pump-down. Personnel access is excluded in all areas affected by operation of the neutron generator.

4.3 Experimental Operations State

All equipment is operational. ITER will be in operation. Personnel access is excluded, according to project safety requirements.

4.4 Maintenance State

ITER is not in operation. Access to equipment for maintenance activities is determined according to project safety requirements. Basically equipment inside the biological shield are maintenance free.

5. CRITICAL DESIGN AREAS AND R&D ITEMS

5.1 Critical Design Areas

- Analysis of the electro-magnetic stress in disruption should be done.

- Effect of the temperature on the sensitivity should be evaluated.

- The technique of the sensitivity calibration should be designed. One of the candidate is putting a small amount of radio active neutron source such as ^{252}Cf near the micro fission chamber. Another candidate is a cross calibration to the neutron activation measurement which is a absolute neutron flux measurement.

5.2 Necessary R&D Items

- The effect of the strong magnetic field on the micro fission chamber should be confirmed experimentally.

- Also effect of the temperature on the sensitivity should be evaluated experimentally.

- Vibration test on the micro fission chamber should be done to simulate the mechanical shock in disruption.

- The effect of the strong RF heating on the micro fission chamber should be confirmed experimentally.

6. CONCLUSION

We designed a neutron monitor using micro fission chambers to be installed inside the vacuum vessel. We investigated the responses of the micro fission chambers to find the suitable position of micro fission chambers by a neutron Monte Carlo calculation using MCNP version 4b code. It was found that the average output of the micro fission chambers at the proposed locations behind blanket modules is insensitive to the changes in the plasma position and the neutron source profile. A set of ^{235}U micro fission chamber and "blank" detector which is a fissile material free detector to identify noise issues such as from gamma-rays are installed behind blankets #11 and #16 in a toroidal location. We propose two toroidal locations for the redundancy.

Employing both pulse counting mode and Campbelling mode in the electronics, we can accomplish the ITER requirement of 10^4 dynamic range with 1 ms temporal resolution. Life time of the micro fission chamber is estimated. The change of the sensitivity is estimated to be only 0.1 % behind blankets for the ITER life time which is equivalent to 0.5 GW•year. So we can use ^{235}U chambers without replacement in the ITER lifetime.

We simulated the *in-situ* calibration by MCNP calculation, where a point source of 14 MeV neutrons is moving on the plasma axis. It was found that the direct calibration was possible by using a neutron generator with an intensity of 10^{11} n/s. The micro fission chamber system can meet the required 10% accuracy for a fusion power monitor.

ACKNOWLEDGMENTS

The authors would like to appreciate Mr. H. Kawasaki and Mr. M. Wada for his support on the neutronics calculations. We appreciate Dr. S. Yamamoto for his pioneer work on the micro fission chambers in ITER CDA.

This report has been prepared as an account of work assigned to the Japanese Home Team under Task Agreement number N 55 TD 02.03 FJ within the Agreement among the European Atomic Energy Community, the Government of Japan, and the Government of the Russian Federation on Cooperation in the Engineering Design Activities for the International Thermonuclear Experimental Reactor ("ITER EDA Agreement") under the auspices of the International Atomic Energy Agency (IAEA).

REFERENCES

[1] O.N. Jarvis, G. Sadler, P. van Bell and T. Elevant: "In-vessel calibration of the JET neutron monitors using a ^{252}Cf neutron source: Difficulties experienced", Rev. Sci. Instrum. **61**, 3172 (1990).

[2] H.W. Hendel, R.W. Palladino, Cris W. Barnes, et al.: "In situ calibration of TFTR neutron detectors", Rev. Sci. Instrum. **61**, 1900 (1990).

[3] T. Nishitani, H. Takeuchi, T. Kondoh, et al.: "Absolute calibration of the JT-60U neutron monitors using a ^{252}Cf neutron source", Rev. Sci. Instrum. **63**, 5270 (1992).

[4] V.Mukhovatov, H. Hopman, S. Yamamoto, et al.: "ITER Diagnostics", ITER Documentation Series, No.33, IAEA, Vienna (1991).

[5] T. Iguchi, J. Kaneko, M. Nakazawa, T. Matoba, T. Nishitani and S. Yamamoto: "Conceptional design of neutron diagnostics system for fusion experimental reactor", Fusion Eng. Design **28**, 689 (1995).

[6] T. Nishitani, K. Ebisawa, T. Iguchi and T. Matoba: "Design of ITER neutron yield monitor using microfission chambers", Fusion Eng. Design **34-35**, 567 (1997).

[7] T. Nishitani, K. Ebisawa, L.C. Johnson, et al.: "In-Vessel Neutron Monitor Using Micro Fission Chambers for ITER", in Diagnostics for Experimental Thermonuclear Fusion Reactor 2, P.E. Stott, G. Gorini and E. Sindoni ed., Plenum Press, New York (1998).

[8] T. Nishitani, S. Kasai, L.C. Johnson, K. Ebisawa, C. Walker and T. Ando: "Neutron monitor using microfission chambers for the International Thermonuclear Fusion Reactor", Rev. Sci. Instrum. **70**, 1141 (1999).

[9] Y. Endo, T. Ito and E. Seki: "A counting-Cambelling neutron measurement system and its experimental results by test reactor", IEEE Trans. Nucl. Sci. **NS-29**, 714 (1982).

[10] J. F. Briesmeister (Ed.): "MCNP - A General Monte Carlo N-Particle Transport Code, version 4B," LA-12625-M, Version 4B, Los Alamos National Laboratory (1997).

[11] T. Nakagawa, K. Shibata, S. Chiba, et al.: "Japanese evaluated nuclear data library version 3 revision-2: JENDL-3.2", J. Nucl. Sci. Technol. **32**, 1259(1995).

[12] Yu.A. Kaschuck, D.V. Portnov, A.V. Krasilnokov, et al.: "Compact Neutron Generator for Diagnostic Applications", Rev. Sci. Instrum. **70**, 1104 (1999).

APPENDIX

Input file of MCNP-4b code for the micro fission chamber response calculation.

```
Iter-feat RESPONSE FUNCTION CALCULATE SPECTRUM.
C    CELL CARDS
c
c   plazma
c
   1   1  1.000e-11   (251  260 -1006 -3) : (-261 1006 -1020)
       : (-271 1020 -1060 251) : (-281 1060 -1050 251) : (-291 1050 1080)
       : (-301 -1080 2 ) : (-311 -260  -2 )
c
c   blanket shield
c
  11   3  1.2366e-1  -251   252   260 -1006
  12   3  1.2366e-1   261  -262  1006 -1020    #(602 -603 ) #(942 -943)
  13   3  1.2366e-1   271  -272  1020 -1060
  14   3  1.2366e-1   281  -282  1060 -1050    #(952 -953 -288)
  15   3  1.2366e-1   291  -292  1050  1080    #(972  973 -298)
  16   3  1.2366e-1   301  -302 -1080    2    #(-992 993 -308)
  17   3  1.2366e-1   311  -312  -260   -2    #(-260 -573 -318)
c
  21  15  8.4488e-2  -252   253   260 -1006
  22  15  8.4488e-2   262  -263  1006 -1020    #(602 -603 ) #(942 -943)
  23  15  8.4488e-2   272  -273  1020 -1060
  24  15  8.4488e-2   282  -283  1060 -1050    #(952 -953 -288)
  25  15  8.4488e-2   292  -293  1050  1080    #(972  973 -298)
  26  15  8.4488e-2   302  -303 -1080    2    #(-992 993 -308)
  27  15  8.4488e-2   312  -313  -260   -2    #(-260 -573 -318)
c
  31  16  8.8116e-2  -253   254   260 -1006
  32  16  8.8116e-2   263  -264  1006 -1020    #(602 -603 ) #(942 -943)
  33  16  8.8116e-2   273  -274  1020 -1060
  34  16  8.8116e-2   283  -284  1060 -1050    #(952 -953 -288)
  35  16  8.8116e-2   293  -294  1050  1080    #(972  973 -298)
  36  16  8.8116e-2   303  -304 -1080    2    #(-992 993 -308)
  37  16  8.8116e-2   313  -314  -260   -2    #(-260 -573 -318)
c
  41  16  8.8116e-2  -254   255   260 -1006
  42  16  8.8116e-2   264  -265  1006 -1020    #(602 -603 ) #(942 -943)
  43  16  8.8116e-2   274  -275  1020 -1060
  44  16  8.8116e-2   284  -285  1060 -1050    #(952 -953 -288)
  45  16  8.8116e-2   294  -295  1050  1080    #(972  973 -298)
  46  16  8.8116e-2   304  -305 -1080    2    #(-992 993 -308)
  47  16  8.8116e-2   314  -315  -260   -2    #(-260 -573 -318)
c
```

```
 51  16 8.8116e-2 -255  256  260 -1006
 52  16 8.8116e-2  265 -266 1006 -1020     #(602 -603 ) #(942 -943)
 53  16 8.8116e-2  275 -276 1020 -1060
 54  16 8.8116e-2  285 -286 1060 -1050     #(952 -953 -288)
 55  16 8.8116e-2  295 -296 1050 1080      #(972  973 -298)
 56  16 8.8116e-2  305 -306 -1080   2     #(-992 993 -308)
 57  16 8.8116e-2  315 -316 -260   -2     #(-260 -573 -318)
c
 61  16 8.8116e-2 -256  258  260 -1006
 62  16 8.8116e-2  266 -268 1006 -1020     #(602 -603) #(942 -943)
 63  16 8.8116e-2  276 -278 1020 -1060
 64  16 8.8116e-2  286 -288 1060 -1050     #(952 -953 -288)
 65  16 8.8116e-2  296 -298 1050 1080      #(972  973 -298)
 66  16 8.8116e-2  306 -308 -1080   2 -1091 #(-992 993 -308)
 67  16 8.8116e-2  316 -318 -260   -2      #(-260 -573 -318)
c
c   gap between blanket and V.V
 71   0          -258 1010  260 -1006
 72   0           268 -1021 1006 -1020
 73   0           278 -1061 1020 -1060
 74   0           288 -1071 1060 -1050
 75   0           298 -1081 1050 1080
 76   0           308   2
      ((-1091 -1080 1090) : (-1121 -1090 1120) : (-1130 -1120 ))
 77   0           318   -2
      ((-1130 -1120 -1002) : (1010 1002 -260))
c
c
 81  16 8.8116e-2 -570 -571 311  -317
 82  16 8.8116e-2  600 -601 261  -267
 83  16 8.8116e-2  940 -941 261  -267
 84  16 8.8116e-2  950 -951 281  -287
 85  16 8.8116e-2  970  971 291  -297
 86  16 8.8116e-2 -990  991 301  -307
c
 91   0          -260 -573 311 -318 #81
 92   0           602 -603 261 -268 #82
 93   0           942 -943 261 -268 #83
 94   0           952 -953 281 -288 #84
 95   0           972  973 291 -298 #85
 96   0          -992  993 301 -308 #86
c
c   vacuum vessele
c
101  12 8.6050e-2 -1010 1011   1002 -1006
102  12 8.6050e-2  1021 -1022  1006 -1020
103  12 8.6050e-2  1061 -1062  1020 -1060
104  12 8.6050e-2  1071 -1072  1060 -1050
105  12 8.6050e-2  1081 -1082  1050 1080
```

```
 106  12 8.6050e-2  1091 -1092   -1080 1090
 107  12 8.6050e-2  1121 -1122   -1090 1120
 108  12 8.6050e-2  1130 -1131   -1120 -1002
c
 111   2 9.5284e-2 -1011  1012   1002 -1006
 112   2 9.5284e-2  1022 -1023   1006 -1020
 113   2 9.5284e-2  1062 -1063   1020 -1060
 114   2 9.5284e-2  1072 -1073   1060 -1050
 115   2 9.5284e-2  1082 -1083   1050  1080
 116   2 9.5284e-2  1092 -1093  -1080 1090
 117   2 9.5284e-2  1122 -1123  -1090 1120
 118   2 9.5284e-2  1131 -1132  -1120 -1002
c
 121  12 8.6050e-2 -1012  1013   1002 -1006
 122  12 8.6050e-2  1023 -1024   1006 -1020
 123  12 8.6050e-2  1063 -1064   1020 -1060
 124  12 8.6050e-2  1073 -1074   1060 -1050
 125  12 8.6050e-2  1083 -1084   1050  1080
 126  12 8.6050e-2  1093 -1094   -1080 1090
 127  12 8.6050e-2  1123 -1124   -1090 1120
 128  12 8.6050e-2  1132 -1133   -1120 -1002
 999   0          (-1013 1002 -1006) : (1024 1006 -1020)
       : (1064 1020 -1060) : (1074 1060 -1050) : (1084 1050 1080)
       : (1094 -1080 1090) : (1124 -1090 1120) : (1133 -1120 -1002)

C    surface cards
   1 tz 0.0 0.0  53.0   620.0   350.0   210.0
   2 cz 508.11
   3 cz 620.0
c
c   blanket shield
 251 cz 406.211
 252 cz 405.211
 253 cz 403.011
 254 cz 391.211
 255 cz 381.211
 256 cz 371.211
 257 cz 363.211
 258 cz 361.211
 260 pz -153.6
c
 261 tz 0.0 0.0 355.004 517.029 110.82  110.82
 262 tz 0.0 0.0 355.004 517.029 111.82  111.82
 263 tz 0.0 0.0 355.004 517.029 114.02  114.02
 264 tz 0.0 0.0 355.004 517.029 125.82  125.82
 265 tz 0.0 0.0 355.004 517.029 135.82  135.82
 266 tz 0.0 0.0 355.004 517.029 145.82  145.82
 267 tz 0.0 0.0 355.004 517.029 153.82  153.82
 268 tz 0.0 0.0 355.004 517.029 155.82  155.82
```

```
c
 271  z 377.240  671.343 443.390 583.876
 272  z 378.038  671.946 444.188 584.479
 273  z 379.793  673.273 445.943 585.806
 274  z 389.204  680.391 455.354 592.924
 275  z 397.180  686.423 463.330 598.956
 276  z 405.156  692.455 471.306 604.988
 277  z 411.536  697.281 477.686 609.814
 278  z 413.132  698.487 479.282 611.020
c
 281 tz 0.0 0.0  17.534 399.298 451.0   451.0
 282 tz 0.0 0.0  17.534 399.298 452.0   452.0
 283 tz 0.0 0.0  17.534 399.298 454.2   454.2
 284 tz 0.0 0.0  17.534 399.298 466.0   466.0
 285 tz 0.0 0.0  17.534 399.298 476.0   476.0
 286 tz 0.0 0.0  17.534 399.298 486.0   486.0
 287 tz 0.0 0.0  17.534 399.298 494.0   494.0
 288 tz 0.0 0.0  17.534 399.298 496.0   496.0
c
 291 tz 0.0 0.0  49.098 596.688 251.1   251.1
 292 tz 0.0 0.0  49.098 596.688 252.1   252.1
 293 tz 0.0 0.0  49.098 596.688 254.3   254.3
 294 tz 0.0 0.0  49.098 596.688 266.1   266.1
 295 tz 0.0 0.0  49.098 596.688 276.1   276.1
 296 tz 0.0 0.0  49.098 596.688 286.1   286.1
 297 tz 0.0 0.0  49.098 596.688 294.1   294.1
 298 tz 0.0 0.0  49.098 596.688 296.1   296.1
c
 301 tz 0.0 0.0  88.177 508.11  425.387 336.811
 302 tz 0.0 0.0  88.177 508.11  426.387 337.811
 303 tz 0.0 0.0  88.177 508.11  428.587 340.011
 304 tz 0.0 0.0  88.177 508.11  440.387 351.811
 305 tz 0.0 0.0  88.177 508.11  450.387 361.811
 306 tz 0.0 0.0  88.177 508.11  460.387 371.811
 307 tz 0.0 0.0  88.177 508.11  468.387 379.811
 308 tz 0.0 0.0  88.177 508.11  470.387 381.811
c
 311 tz 0.0 0.0 -153.6  508.11  183.611 101.899
 312 tz 0.0 0.0 -153.6  508.11  184.611 102.899
 313 tz 0.0 0.0 -153.6  508.11  186.811 105.099
 314 tz 0.0 0.0 -153.6  508.11  198.611 116.899
 315 tz 0.0 0.0 -153.6  508.11  208.611 126.899
 316 tz 0.0 0.0 -153.6  508.11  218.611 136.899
 317 tz 0.0 0.0 -153.6  508.11  226.611 144.899
 318 tz 0.0 0.0 -153.6  508.11  228.611 146.899
c
c
c filler-1
 570 pz -155.6
```

```
 571  z -159.5   383.2  -169.7   357.2
 573  z -161.362 383.93 -171.562 357.93
c filler-2
 600 pz  402.4
 601  z  405.7   407.0   437.7   380.3
 602 pz  400.4
 603  z  406.981 408.536 438.981 381.836
c filler-4
 940  z  502.4   578.9   466.2   574.8
 941  z  492.1   599.1   464.8   578.4
 942  z  502.625 576.913 466.425 572.813
 943  z  490.892 600.694 463.592 579.994
c filler-5
 950  z  349.4   773.3   332.7   757.6
 951  z  341.3   780.3   329.6   760.1
 952  z  350.77  771.843 334.070 756.143
 953  z  339.569 781.302 327.869 761.102
c filler-7
 970  z  81.1    895.1    76.1   868.1
 971  z  67.4    896.2    72.2   868.1
 972  z  83.067  894.736  78.067 867.736
 973  z  65.429  895.863  70.229 867.763
c filler-9
 990  z -256.6   765.7   -242.3   740.8
 991  z -267.8   755.8   -245.3   738.2
 992  z -254.866 766.696 -240.566 741.796
 993  z -269.032 754.225 -246.532 736.625
c
c  surfce of tally
1201  tz  0.0  0.0 -213.300  366.308  20.0  20.0
1202  tz  0.0  0.0 -100.725  361.211  20.0  20.0
1203  tz  0.0  0.0  16.9000  361.211  20.0  20.0
1204  tz  0.0  0.0  124.425  361.211  20.0  20.0
1205  tz  0.0  0.0  237.000  361.211  20.0  20.0
1206  tz  0.0  0.0  335.000  361.211  20.0  20.0
1207  tz  0.0  0.0  474.000  416.432  20.0  20.0
1208  tz  0.0  0.0  509.550  536.914  20.0  20.0
1209  tz  0.0  0.0  465.113  629.755  20.0  20.0
1210  tz  0.0  0.0  385.125  732.304  20.0  20.0
1211  tz  0.0  0.0  305.138  803.402  20.0  20.0
1212  tz  0.0  0.0  231.075  846.977  20.0  20.0
c  1213  tz  0.0  0.0  130.350  881.422  20.0  20.0
1213  tz  0.0  0.0  130.350  882.298  20.0  20.0
1214  tz  0.0  0.0   11.900  890.442  20.0  20.0
c  1215  tz  0.0  0.0 -112.575  853.403  20.0  20.0
1215  tz  0.0  0.0 -110.000  854.381  20.0  20.0
1216  tz  0.0  0.0 -204.413  807.069  20.0  20.0
1217  tz  0.0  0.0 -302.000  721.364  20.0  20.0
c   vacuum vessele
```

```
1002 pz -355.185
1006 pz  355.004
1020  z  355.004  517.029  482.472  613.433
1060  z   17.534  399.298  416.322  700.9
1050  z   17.534  399.298  108.349  967.228
1080  z  -72.036  871.252   49.098  596.688
1090  z -364.435  742.249 -263.525  513.522
1120  z -513.463  518.987 -263.525  513.522
c
1010 cz 357.211
1011 cz 351.211
1012 cz 345.211
1013 cz 339.211
1021 tz 0.0 0.0 355.004  517.029  159.820  159.820
1022 tz 0.0 0.0 355.004  517.029  165.820  165.820
1023 tz 0.0 0.0 355.004  517.029  171.820  171.820
1024 tz 0.0 0.0 355.004  517.029  177.820  177.820
1061  z 416.322   700.9   482.472  613.433
1062  z 421.112   704.520 487.262  617.053
1063  z 425.893   708.138 492.043  620.671
1064  z 430.679   711.758 496.829  624.291
1071 tz 0.0 0.0  17.534  399.298  500.0   500.0
1072 tz 0.0 0.0  17.534  399.298  506.0   506.0
1073 tz 0.0 0.0  17.534  399.298  512.0   512.0
1074 tz 0.0 0.0  17.534  399.298  518.0   518.0
1081 tz 0.0 0.0  49.098  596.688  300.1   300.1
1082 tz 0.0 0.0  49.098  596.688  306.1   306.1
1083 tz 0.0 0.0  49.098  596.688  312.1   312.1
1084 tz 0.0 0.0  49.098  596.688  318.1   318.1
1091  z -364.435  742.249  -72.036  871.252
1092  z -366.856  747.739  -74.457  876.742
1093  z -369.279  753.228  -76.880  882.231
1094  z -371.701  758.717  -79.302  887.720
1121 tz 0.0 0.0 -263.525  513.522  250.0   250.0
1122 tz 0.0 0.0 -263.525  513.522  256.0   256.0
1123 tz 0.0 0.0 -263.525  513.522  262.0   262.0
1124 tz 0.0 0.0 -263.525  513.522  268.0   268.0
1130 tz 0.0 0.0 -355.185  515.526  158.32  158.32
1131 tz 0.0 0.0 -355.185  515.526  164.32  164.32
1132 tz 0.0 0.0 -355.185  515.526  170.32  170.32
1133 tz 0.0 0.0 -355.185  515.526  176.32  176.32

C     PROBREM TYPE CARD
mode n
c     imp:n 1  99r 0
c   * weight windows.
 wwn1:n  0.0  0.9 6r  0.8  6r  0.5  6r  0.1  6r  0.05  6r  0.01  6r  0.0  6r
       0.0   5r  0.0  5r
       5.0-3  7r  0.01  7r  0.1  7r
```

```
     -1
 wwp:n  5 3 5 0 0
C   material data
c
c  vacuum (t.a.d = 1.0e-11)
c
 m1  1001.37c  1.0
c
c  SS-Borated  (ASTM-A887-89...60%,H2O...40%)
c                t.a.d = 9.5284e-02
c
 m2  5010.37c 1.1334e-03  5011.37c 4.1232e-03  6012.37c 1.8894e-04
     7014.37c 2.0256e-04 14000.37c 7.5780e-04 15031.37c 4.1214e-05
    16000.37c 2.6538e-05 24000.37c 1.0368e-02 25055.37c 1.0326e-03
    26000.37c 3.0732e-02 28000.37c 6.5280e-03  1001.37c 2.6764e-02
     8016.37c 1.3386e-02
mt2  lwtr.01t  $ 300K
c
c  Be...100%   (t.a.d = 1.2366e-01)
c
 m3  4009.37c 1.2366e-01
c
c  S.S.316ln...100%
c                t.a.d = 8.6050e-02
c
 m12 5010.37c 8.7458e-07  5011.37c 3.5430e-06  6012.37c 8.9470e-05
     7014.37c 2.3870e-04  8016.37c 5.9710e-06 13027.37c 8.8510e-05
    14000.37c 8.5030e-04 15031.37c 3.8550e-05 16000.37c 1.1173e-05
    19000.37c 6.1080e-07 22000.37c 1.4960e-04 23051.37c 3.7500e-06
    24000.37c 1.6070e-02 25055.37c 1.5650e-03 26000.37c 5.5600e-02
    27059.37c 4.0520e-05 28000.37c 9.9690e-03 29000.37c 7.5161e-05
    40000.37c 1.0470e-06 41093.37c 2.5703e-06 42000.37c 1.2450e-03
    50000.01c 8.0470e-07 73181.37c 2.6400e-07 74000.37c 2.5980e-07
    82000.37c 1.8440e-07 83209.37c 1.8280e-07
c
c  First wall (Cu..74.30%, H2O..17.80%,  S.S.316ln...7.90%)
c                t.a.d = 8.4488e-02
c
 m15 5010.37c 6.9092e-08  5011.37c 2.7990e-07  6012.37c 7.0681e-06
     7014.37c 1.8857e-05  8016.37c 4.7171e-07 13027.37c 6.9923e-06
    14000.37c 6.7174e-05 15031.37c 3.0455e-06 16000.37c 8.8264e-07
    19000.37c 4.8253e-08 22000.37c 1.1818e-05 23051.37c 2.9625e-07
    24000.37c 1.2696e-03 25055.37c 1.2364e-04 26000.37c 4.3924e-03
    27059.37c 3.2011e-06 28000.37c 7.8754e-04 29000.37c 5.9376e-06
    40000.37c 8.2713e-08 41093.37c 2.0305e-07 42000.37c 9.8355e-05
    50000.01c 6.3571e-08 73181.37c 2.0856e-08 74000.37c 2.0524e-08
    82000.37c 1.4568e-08 83209.37c 1.4441e-08
     1001.37c 1.0719e-02  8016.37c 5.3613e-03 29000.37c 6.1609e-02
mt15 lwtr.01t  $ 300K
```

```
c
c  blanket shield  (H2O..20.00%,  S.S.316ln..80.00%)
c                  t.a.d = 8.8116e-02
c
 m16  5010.37c 6.9966e-07  5011.37c 2.8344e-06  6012.37c 7.1576e-05
     7014.37c 1.9096e-04  8016.37c 4.7768e-06 13027.37c 7.0808e-05
    14000.37c 6.8024e-04 15031.37c 3.0840e-05 16000.37c 8.9381e-06
    19000.37c 4.8864e-07 22000.37c 1.1968e-04 23051.37c 3.0000e-06
    24000.37c 1.2856e-02 25055.37c 1.2520e-03 26000.37c 4.4480e-02
    27059.37c 3.2416e-05 28000.37c 7.9752e-03 29000.37c 6.0127e-05
    40000.37c 8.3760e-07 41093.37c 2.0562e-06 42000.37c 9.9600e-04
    50000.01c 6.4376e-07 73181.37c 2.1120e-07 74000.37c 2.0784e-07
    82000.37c 1.4752e-07 83209.37c 1.4624e-07
     1001.37c 1.3383e-02  8016.37c 6.6932e-03
mt16 lwtr.01t   $ 300K
 m235 92235.37c  1.0
c
C    TALLY
 E0     1.00-6   2.15-6   4.65-6   1.00-5   2.15-5   4.65-5
        1.00-4   2.15-4   4.65-4   1.00-3   2.15-3   4.65-3
        1.00-2   2.15-2   4.65-2   1.00-1   1.41-1   2.00-1
        2.83-1   4.00-1   5.66-1   8.00-1   1.058    1.400
        1.871    2.500    3.162    4.000    4.516    5.099
        5.757    6.500    7.328    8.261    9.314    10.50
        11.478   12.549   13.720   15.000
c
 f12:n 318
 fs12  1201
 sd12  1.0   9.21264e+4
c
 f22:n 258
 fs22  1202
 sd22  1.0   9.07822e+4
c
 f32:n 258
 fs32  1203
 sd32  1.0   9.07822e+4
c
 f42:n 258
 fs42  1204
 sd42  1.0   9.07822e+4
c
 f52:n 258
 fs52  1205
 sd52  1.0   9.07822e+4
c
 f62:n 258
 fs62  1206
 sd62  1.0   9.07822e+4
```

```
c
 f72:n 268
 fs72  1207
 sd72  1.0   1.04802e+5
c
 f82:n 268
 fs82  1208
 sd82  1.0   1.35020e+5
c
 f92:n 278
 fs92  1209
 sd92  1.0   1.58275e+5
c
 f102:n 288
 fs102  1210
 sd102  1.0   1.84038e+5
c
 f112:n 288
 fs112  1211
 sd112  1.0   2.01903e+5
c
 f122:n 288
 fs122  1212
 sd122  1.0   2.12852e+5
c
 f132:n 288
 fs132  1213
 sd132  1.0   2.21728e+5
c
 f142:n 298
 fs142  1214
 sd142  1.0   2.23792e+5
c
 f152:n 308
 fs152  1215
 sd152  1.0   1.19056e+5
c
 f162:n 308
 fs162  1216
 sd162  1.0   2.02824e+5
c
 f172:n 308
 fs172  1217
 sd172  1.0   1.81291e+5
c
c
 fm12 ( 1.0  235 (-6))
 fm22 ( 1.0  235 (-6))
 fm32 ( 1.0  235 (-6))
```

```
fm42 ( 1.0  235 (-6))
fm52 ( 1.0  235 (-6))
fm62 ( 1.0  235 (-6))
fm72 ( 1.0  235 (-6))
fm82 ( 1.0  235 (-6))
fm92 ( 1.0  235 (-6))
fm102 ( 1.0  235 (-6))
fm112 ( 1.0  235 (-6))
fm122 ( 1.0  235 (-6))
fm132 ( 1.0  235 (-6))
fm142 ( 1.0  235 (-6))
fm152 ( 1.0  235 (-6))
fm162 ( 1.0  235 (-6))
fm172 ( 1.0  235 (-6))
c
C     SOURCE CARDS (ISOTROPIC PROFILE SOURCE DT NEUTRON)
rdum  620.0  170.0  1.7  53.0 1.3  14.1  0.35  0.5
c
cut:n  1.0E25  5.5E-7 -0.5 -0.25 0
phys:n  15.0  5.5E-7
nps  90000000
ctme  200
lost 100 5
C
prdmp  j  -100  1 3
PRINT -175
```

This is a blank page.

国際単位系 (SI) と換算表

表 1　SI基本単位および補助単位

量	名称	記号
長さ	メートル	m
質量	キログラム	kg
時間	秒	s
電流	アンペア	A
熱力学温度	ケルビン	K
物質量	モル	mol
光度	カンデラ	cd
平面角	ラジアン	rad
立体角	ステラジアン	sr

表 2　SIと併用される単位

名称	記号
分，時，日	min，h，d
度，分，秒	°，′，″
リットル	l，L
トン	t
電子ボルト	eV
原子質量単位	u

1 eV = 1.60218 × 10^{-19} J

1 u = 1.66054 × 10^{-27} kg

表 5　SI接頭語

倍数	接頭語	記号
10^{18}	エクサ	E
10^{15}	ペタ	P
10^{12}	テラ	T
10^{9}	ギガ	G
10^{6}	メガ	M
10^{3}	キロ	k
10^{2}	ヘクト	h
10^{1}	デカ	da
10^{-1}	デシ	d
10^{-2}	センチ	c
10^{-3}	ミリ	m
10^{-6}	マイクロ	μ
10^{-9}	ナノ	n
10^{-12}	ピコ	p
10^{-15}	フェムト	f
10^{-18}	アト	a

表 3　固有の名称をもつSI組立単位

量	名称	記号	他のSI単位による表現
周波数	ヘルツ	Hz	s^{-1}
力	ニュートン	N	m·kg/s^2
圧力，応力	パスカル	Pa	N/m^2
エネルギー，仕事，熱量	ジュール	J	N·m
工率，放射束	ワット	W	J/s
電気量，電荷	クーロン	C	A·s
電位，電圧，起電力	ボルト	V	W/A
静電容量	ファラド	F	C/V
電気抵抗	オーム	Ω	V/A
コンダクタンス	ジーメンス	S	A/V
磁束	ウェーバ	Wb	V·s
磁束密度	テスラ	T	Wb/m^2
インダクタンス	ヘンリー	H	Wb/A
セルシウス温度	セルシウス度	℃	
光束	ルーメン	lm	cd·sr
照度	ルクス	lx	lm/m^2
放射能	ベクレル	Bq	s^{-1}
吸収線量	グレイ	Gy	J/kg
線量当量	シーベルト	Sv	J/kg

表 4　SIと共に暫定的に維持される単位

名称	記号
オングストローム	Å
バーン	b
バール	bar
ガル	Gal
キュリー	Ci
レントゲン	R
ラド	rad
レム	rem

1 Å = 0.1 nm = 10^{-10} m

1 b = 100 fm^2 = 10^{-28} m^2

1 bar = 0.1 MPa = 10^5 Pa

1 Gal = 1 cm/s^2 = 10^{-2} m/s^2

1 Ci = 3.7 × 10^{10} Bq

1 R = 2.58 × 10^{-4} C/kg

1 rad = 1 cGy = 10^{-2} Gy

1 rem = 1 cSv = 10^{-2} Sv

(注)

1. 表1－5は「国際単位系」第5版，国際度量衡局 1985年刊行による。ただし，1 eVおよび1 uの値はCODATAの1986年推奨値によった。
2. 表4には海里，ノット，アール，ヘクタールも含まれているが日常の単位なのでここでは省略した。
3. barは，JISでは流体の圧力を表わす場合に限り表2のカテゴリーに分類されている。
4. EC閣僚理事会指令ではbar，barnおよび「血圧の単位」mmHgを表2のカテゴリーに入れている。

換算表

力	N(=10^5 dyn)	kgf	lbf
	1	0.101972	0.224809
	9.80665	1	2.20462
	4.44822	0.453592	1

粘度　1 Pa·s(N·s/m^2) = 10 P(ポアズ)(g/(cm·s))

動粘度　1 m^2/s = 10^4 St(ストークス)(cm^2/s)

圧力	MPa(=10 bar)	kgf/cm^2	atm	mmHg(Torr)	lbf/in^2(psi)
	1	10.1972	9.86923	7.50062 × 10^3	145.038
	0.0980665	1	0.967841	735.559	14.2233
	0.101325	1.03323	1	760	14.6959
	1.33322 × 10^{-4}	1.35951 × 10^{-3}	1.31579 × 10^{-3}	1	1.93368 × 10^{-2}
	6.89476 × 10^{-3}	7.03070 × 10^{-2}	6.80460 × 10^{-2}	51.7149	1

エネルギー・仕事・熱量	J(=10^7 erg)	kgf·m	kW·h	cal(計量法)	Btu	ft·lbf	eV
	1	0.101972	2.77778 × 10^{-7}	0.238889	9.47813 × 10^{-4}	0.737562	6.24150 × 10^{18}
	9.80665	1	2.72407 × 10^{-6}	2.34270	9.29487 × 10^{-3}	7.23301	6.12082 × 10^{19}
	3.6 × 10^6	3.67098 × 10^5	1	8.59999 × 10^5	3412.13	2.65522 × 10^6	2.24694 × 10^{25}
	4.18605	0.426858	1.16279 × 10^{-6}	1	3.96759 × 10^{-3}	3.08747	2.61272 × 10^{19}
	1055.06	107.586	2.93072 × 10^{-4}	252.042	1	778.172	6.58515 × 10^{21}
	1.35582	0.138255	3.76616 × 10^{-7}	0.323890	1.28506 × 10^{-3}	1	8.46233 × 10^{18}
	1.60218 × 10^{-19}	1.63377 × 10^{-20}	4.45050 × 10^{-26}	3.82743 × 10^{-20}	1.51857 × 10^{-22}	1.18171 × 10^{-19}	1

1 cal = 4.18605 J (計量法)

= 4.184 J (熱化学)

= 4.1855 J (15 °C)

= 4.1868 J (国際蒸気表)

仕事率　1 PS (仏馬力)

= 75 kgf·m/s

= 735.499 W

放射能	Bq	Ci
	1	2.70270 × 10^{-11}
	3.7 × 10^{10}	1

吸収線量	Gy	rad
	1	100
	0.01	1

照射線量	C/kg	R
	1	3876
	2.58 × 10^{-4}	1

線量当量	Sv	rem
	1	100
	0.01	1

(86年12月26日現在)

Design of In-vessel Neutron Monitor using Micro Fission Chambers for ITER